

# Constraining Nonstandard Neutrino-Electron Interactions due to a New Light Spin-1 Boson

Cheng-Wei Chiang,<sup>a,b,c</sup> Gaber Faisal,<sup>a,d,e</sup> Yi-Fan Lin,<sup>a</sup> and Jusak Tandean<sup>a,e</sup>

<sup>a</sup>*Department of Physics and Center for Mathematics and Theoretical Physics,  
National Central University,  
Chungli 320, Taiwan*

<sup>b</sup>*Institute of Physics, Academia Sinica,  
Taipei 115, Taiwan*

<sup>c</sup>*Physics Division,  
National Center for Theoretical Sciences,  
Hsinchu 300, Taiwan*

<sup>d</sup>*Egyptian Center for Theoretical Physics,  
Modern University for Information and Technology,  
Cairo, Egypt*

<sup>e</sup>*Department of Physics and Center for Theoretical Sciences,  
National Taiwan University,  
Taipei 106, Taiwan*

## Abstract

We consider nonstandard interactions of neutrinos with electrons arising from a new light spin-1 particle with mass of tens of GeV or lower and couplings to the neutrinos and electron. This boson is not necessarily a gauge boson and is assumed to have no mixing with standard-model gauge bosons. Adopting a model-independent approach, we study constraints on the flavor-conserving and -violating couplings of the boson with the leptons from a number of experimental data. Specifically, we take into account the (anti)neutrino-electron scattering and  $e^+e^- \rightarrow \nu\bar{\nu}\gamma$  measurements and keep explicitly the dependence on the new particle mass in all calculations. We find that one of the two sets of data can provide the stronger constraints, depending on the mass and width of the boson. Also, we evaluate complementary constraints on its separate flavor-conserving couplings to the electron and neutrinos from other latest experimental results.

## I. INTRODUCTION

A growing amount of experimental data has now confirmed that neutrinos possess mass and mix among themselves [1]. The masslessness of the neutrinos in the minimal standard model (SM) implies that extra ingredients beyond them are necessary to account for this observation. Despite the accumulating knowledge of neutrino properties, the nature of the mechanism responsible for generating neutrino masses and mixing is still a mystery [1]. It is generally expected, however, that the underlying new physics would also modify the structure of the electroweak neutral and charged currents in the SM. Such modifications in the neutrino sector give rise to the so-called nonstandard interactions (NSI) of the neutrinos [2–4]. In most studies on such NSI, they arise from the exchange of new particles that are usually assumed to be heavier than the electroweak scale and, thus, lead to effective four-fermion interactions for low-energy phenomenology. Nevertheless, it is also feasible that the exchanged new particle is not heavy, *e.g.*, in the GeV or sub-GeV regime. One of the simplest possibilities along this line is that the new particle is a spin-1 boson.

Scenarios beyond the SM involving new spin-1 particles with relatively low masses have been considered to some extent in various contexts in the literature. Generally speaking, their existence is not just still compatible with current data, but also highly desirable, as they may offer explanations for some of the recent experimental anomalies and unexpected observations. For instance, a spin-1 boson having a mass of a few GeV and interactions with both quarks and leptons has been proposed to explain the measured value of the muon  $g-2$  and the NuTeV anomaly simultaneously [5, 6], although the latter may now be explicable by taking into account the appropriate nuclear effects [7, 8]. As another example, an  $\mathcal{O}(\text{MeV})$  spin-1 boson which couples to dark matter as well as leptons may be the cause of the observed 511-keV emission from the bulge of our galaxy [9, 10]. If its mass is at the GeV level, such a particle may be associated with the unexpected excess of positrons seen in cosmic rays, potentially attributable to dark-matter annihilation [11]. In the context of hyperon decays, a spin-1 boson with mass around 0.2 GeV, flavor-changing couplings to quarks, and a primary decay channel into  $\mu^+\mu^-$  can account for the three anomalous events of  $\Sigma^+ \rightarrow p\mu^+\mu^-$  detected in the HyperCP experiment several years ago [12]. Lastly, a spin-1 particle lighter than the  $b$  quark could be responsible [13] for the unexpectedly sizable like-sign dimuon charge asymmetry in semileptonic  $b$ -hadron decays recently reported by the DØ Collaboration [14]. Although in these few instances the spin-1 particles tend to have suppressed couplings to SM particles, it is possible to test their existence or effects in future high-precision experiments [9, 11–13, 15, 16].

In the present paper, we explore the possibility that a nonstandard spin-1 boson under 100 GeV is electrically neutral, carries no color, and has couplings to both the neutrinos and electron. Consequently, it will affect processes that involve at least these leptons. In particular, we will focus on such processes for which plenty of experimental data are available. In our study, the new particle, to which we refer as the  $X$  boson, is not necessarily a gauge boson. Therefore, its couplings to the leptons are kept sufficiently general for a model-independent analysis. The results of our analysis can be readily applied to the specific case where  $X$  is a gauge boson or any model with definite couplings of  $X$ . For simplicity, we also assume that the  $X$  boson does not mix with the SM gauge bosons, *i.e.*,  $Z$  and  $\gamma$ . As alluded to earlier, most previous NSI studies concentrate on the scenario of heavy new particles. As far as we know, the low-mass effects of  $X$

on the determination of its couplings have not been studied in detail before. When the mass of  $X$  is close to the momenta exchanged in a scattering process, both the exchanged momenta and the  $X$ -boson mass (and even its total decay width) have to be kept in the calculations. This work is complementary to analyses on neutrino NSI due to new physics above the electroweak scale (*e.g.*, Refs. [2–4]).

The structure of this paper is organized as follows. In the next section, we write down an interaction Lagrangian for  $X$  with the leptons and subsequently describe the (anti)neutrino-electron and  $e^+e^- \rightarrow \nu\bar{\nu}\gamma$  scattering processes that will be used to constrain possible values of the  $X$  couplings to the leptons. From Section III to Section VII, we concentrate on the flavor-conserving interactions. In Sections III and IV, we extract constraints on the  $X$  couplings to the electron and to the electron neutrino and antineutrino from the low-energy  $\nu_e e \rightarrow \nu e$  and  $\bar{\nu}_e e \rightarrow \bar{\nu} e$  data, respectively. A combined result from the two sets of data is presented at the end of Section IV. Section V deals with the bounds on the  $X$  couplings to the electron and to the muon neutrinos based on the CHARM-II data. In Section VI, the data on  $e^+e^- \rightarrow \nu\bar{\nu}\gamma$  cross-section collected by the ALEPH, DELPHI, L3, and OPAL Collaborations are employed to restrict the leptonic couplings of  $X$ , with several illustrative choices of its mass and total decay width. We also discuss the complementarity of the (anti)neutrino-electron and  $e^+e^- \rightarrow \nu\bar{\nu}\gamma$  measurements in probing these couplings. Since the  $X$  contributions to these observables always involve the products of its respective couplings to the electron and neutrinos, the resulting constraints also apply only to the products, instead of the individual couplings. It is therefore of interest to determine constraints on the separate couplings making use of other experimental information, which is also available. We pursue this in Section VII for the flavor-conserving couplings employing  $e^+e^-$  collision data at the  $Z$ -pole, the measured anomalous magnetic moment of the electron, and the results of searches for a nonstandard spin-1 particle at fixed-target and beam-dump experiments. Comparing the various results would allow us to see which observables are most sensitive to the different  $X$  couplings. Finally, in Section VIII we address constraints on the couplings for the flavor-changing  $X$ -neutrino interactions from the same sets of experimental data utilized in Sections III–VI. Our findings are summarized in Section IX. Some longer formulas are collected in an appendix.

## II. INTERACTIONS AND CROSS SECTIONS

The Lagrangian describing the effective interactions of  $X$  with the neutrinos,  $\nu_i$ , and electron,  $e$ , can take the form

$$\mathcal{L}_X = -g_{\nu_i\nu_j} \bar{\nu}_i \gamma^\beta P_L \nu_j X_\beta - \bar{e} \gamma^\beta (g_{Le} P_L + g_{Re} P_R) e X_\beta, \quad (1)$$

where summation over  $i, j = e, \mu, \tau$  is implied, we have allowed for the possibility of  $X$ -induced neutrino flavor-change, and  $P_{L,R} = \frac{1}{2}(1 \mp \gamma_5)$ . Since presently there is still no compelling evidence for the existence of predominantly right-handed neutrinos [17], we have neglected their potential couplings to  $X$ . We also have not included terms involving the muon or tau, as the electron is the only charged lepton taking part in the reactions we will study. The Hermiticity of  $\mathcal{L}_X$  implies that  $g_{\nu_i\nu_j} = g_{\nu_j\nu_i}^*$  and that  $g_{Le,Re}$  are real. In our model-independent approach, we assume that these parameters are free and can be family nonuniversal. We further assume that additional coupling constants which  $X$  may have parametrizing its interactions, flavor-conserving and/or

flavor-violating, with other fermions already satisfy the experimental constraints to which the couplings are subject, but which we do not address in this paper.

In the SM, neutrino-electron interactions proceed from diagrams with the  $W$  and  $Z$  bosons exchanged between the fermions. The relevant Lagrangian is given by

$$\mathcal{L}_{\text{SM}} = -\frac{g}{\sqrt{2}}(\bar{\nu}_e \gamma^\beta P_L e W_\beta^+ + \text{H.c.}) - \frac{g}{2c_w} \bar{\nu}_i \gamma^\beta P_L \nu_i Z_\beta - \frac{g}{c_w} \bar{e} \gamma^\beta (\bar{g}_L P_L + \bar{g}_R P_R) e Z_\beta, \quad (2)$$

$$\bar{g}_L = -\frac{1}{2} + s_w^2, \quad \bar{g}_R = s_w^2 = \sin^2 \theta_W, \quad c_w = \cos \theta_W, \quad (3)$$

where as usual  $g$  is the weak coupling constant and  $\theta_W$  the Weinberg angle.

One can place bounds on the products of  $X$  couplings to the neutrino and electron in Eq. (1) from the cross sections of  $\nu e \rightarrow \nu e$  and  $\bar{\nu} e \rightarrow \bar{\nu} e$  scattering which have been determined in a number of low-energy experiments [18–27]. The accumulated data are generally consistent with SM expectations, but there is room left for new physics.

In the SM, the amplitude for  $\nu_e e^- \rightarrow \nu_e e^-$  at tree level comes from  $u$ -channel  $W$ -mediated and  $t$ -channel  $Z$ -mediated diagrams, while for  $\nu_\mu e^- \rightarrow \nu_\mu e^-$  the  $W$  contribution is absent [28]. For these processes, the  $X$  interactions in Eq. (1) can induce  $t$ -channel diagrams. The latter type of  $X$ -mediated diagram is the only contribution at leading order to  $\nu_i e^- \rightarrow \nu_j e^-$  for  $j \neq i$  in the absence of other nonstandard mechanisms. Since the final neutrino in the  $\nu e$  scattering experiments is not detected, any one of the three light-neutrino flavors can occur in the final state. It follows that for  $\nu_i e^- \rightarrow \nu e^-$  and  $i = e$  or  $\mu$  we have the differential cross-section

$$\frac{d\sigma_{\nu_i e}}{dT} = \frac{1}{32\pi E_\nu^2 m_e} \sum_{j=e,\mu,\tau} \overline{|\mathcal{M}_{\nu_i e \rightarrow \nu_j e}|^2}, \quad (4)$$

where  $E_\nu$  and  $T$  denote, respectively, the energy of the incident neutrino and the kinetic energy of the recoiling electron both in the laboratory frame,  $m_e$  is the electron mass, and the general expressions for the squared amplitudes can be found in Eqs. (A1)-(A5) in the Appendix.

In the case that the momentum transfers in the scattering are small compared to the  $W$  and  $X$  masses, we can write approximately

$$\frac{d\sigma_{\nu_i e}}{dT} = \frac{d\sigma_{\nu_i e}^{\text{FD}}}{dT} + \frac{d\sigma_{\nu_i e}^{\text{FC}}}{dT}, \quad (5)$$

$$\begin{aligned} \frac{d\sigma_{\nu_i e}^{\text{FD}}}{dT} = \frac{2G_{\text{F}}^2 m_e}{\pi} & \left[ \left( \omega + \bar{g}_L + \frac{L_{ii}}{2\sqrt{2} G_{\text{F}} m_X^2} \right)^2 + \left( \bar{g}_R + \frac{R_{ii}}{2\sqrt{2} G_{\text{F}} m_X^2} \right)^2 \left( 1 - \frac{T}{E_\nu} \right)^2 \right. \\ & \left. - \left( \omega + \bar{g}_L + \frac{L_{ii}}{2\sqrt{2} G_{\text{F}} m_X^2} \right) \left( \bar{g}_R + \frac{R_{ii}}{2\sqrt{2} G_{\text{F}} m_X^2} \right) \frac{m_e T}{E_\nu^2} \right], \end{aligned} \quad (6)$$

$$\frac{d\sigma_{\nu_i e}^{\text{FC}}}{dT} = \frac{m_e}{4\pi m_X^4} \sum_{j \neq i} \left[ |L_{ji}|^2 + |R_{ji}|^2 \left( 1 - \frac{T}{E_\nu} \right)^2 - L_{ij} R_{ji} \frac{m_e T}{E_\nu^2} \right], \quad (7)$$

where the two parts in Eq. (5) arise from flavor-diagonal (FD) and flavor-changing (FC) interactions, respectively,  $G_F = g^2/(32m_W^4)^{1/2}$  as usual,  $\omega = 1$  (0) if  $i = e$  ( $\mu$ ), and  $C_{ij} = g_{\nu_i\nu_j}g_{C_e}$  for  $C = L, R$ , implying that  $C_{ij}^* = C_{ji}$  and  $\text{Re}(L_{ji}^*R_{ji}) = L_{ij}R_{ji}$ . In the  $L_{ii} = R_{ii} = 0$  limit, Eq. (6) reproduces the well-known SM contribution [28]. For  $i = e$  and  $E_\nu \gg m_e$ , we then arrive at

$$\begin{aligned} \sigma_{\nu_e e} = & \frac{2G_F^2 E_\nu m_e}{\pi} \left[ \left( 1 + \bar{g}_L + \frac{L_{ee}}{2\sqrt{2}G_F m_X^2} \right)^2 + \frac{1}{3} \left( \bar{g}_R + \frac{R_{ee}}{2\sqrt{2}G_F m_X^2} \right)^2 \right] \\ & + \frac{E_\nu m_e}{4\pi m_X^4} \left( |L_{\mu e}|^2 + \frac{|R_{\mu e}|^2}{3} + (\mu \rightarrow \tau) \right) \end{aligned} \quad (8)$$

after integration over the  $T$  range in Eq. (A7) and keeping terms to first order in  $m_e$ .

If  $m_X$  is not large compared to the momentum transfer, one needs to employ the general expressions in Eqs. (A1)-(A5) to calculate the cross sections  $\sigma_{\nu_e e}$ , but the approximations such as made in the previous paragraph are still applicable to the SM part for momenta much smaller than  $m_W$ . Moreover, for  $\nu_e e$  scattering with incident neutrinos having been produced in  $\mu^+$  decays at rest and therefore not being monoenergetic, one has to integrate  $\sigma_{\nu_e e}$  over the appropriate  $\nu_e$  spectrum [29]. This results in the flux-averaged cross-section [18]

$$\bar{\sigma}_{\nu_e e} = \int_0^{E_\nu^{\max}} dE_\nu \phi_{\nu_e}(E_\nu) \sigma_{\nu_e e}, \quad (9)$$

where the limits span the  $\nu_e$  energy range in  $\mu^+$  decay,  $E_\nu^{\max} = (m_\mu^2 - m_e^2)/(2m_\mu) \simeq 52.8$  MeV with the  $\nu$  masses neglected, and the spectrum is given by [29]  $\phi_{\nu_e}(E_\nu) = 12(E_\nu^{\max} - E_\nu)E_\nu^2/(E_\nu^{\max})^4$ , which is normalized to unity.

In the  $\bar{\nu}_e e^- \rightarrow \bar{\nu} e^-$  processes of interest, the source of the incident antineutrinos is a nuclear reactor and hence they do not share the same energy. The cross section then again needs to be integrated over the reactor antineutrino spectrum [4, 29],

$$\bar{\sigma}_{\bar{\nu}_e e} = \int_{T_{\min}}^{T_{\max}} dT \int_{E_{\bar{\nu}}^{\min}}^{E_{\bar{\nu}}^{\max}} dE_{\bar{\nu}} \phi_{\bar{\nu}_e}(E_{\bar{\nu}}) \frac{d\sigma_{\bar{\nu}_e e}}{dT}, \quad (10)$$

where  $T_{\min, \max}$  denote the experimental cuts on the kinetic energy  $T$  of the recoiling electron in the lab frame,  $E_{\bar{\nu}}^{\min}$  is a function of  $T$  according to Eq. (A8), and the spectrum, which extends essentially to  $E_{\bar{\nu}}^{\max} \sim 10$  MeV, is given by [3, 4]

$$\phi_{\bar{\nu}_e}(E_{\bar{\nu}}) = \sum_k a_k S_k(E_{\bar{\nu}}), \quad (11)$$

the sum of the spectra  $S_k(E_{\bar{\nu}})$  from isotopes  $k$  with fractional contributions  $a_k$ . The differential cross-section  $d\sigma_{\bar{\nu}_e e}/dT$  for  $m_{W, X}$  large compared to the total energy in this scattering can be derived from Eqs. (5)-(7) by making the interchanges  $1 + \bar{g}_L \leftrightarrow \bar{g}_R$  and  $L_{ij} \leftrightarrow R_{ij}$ . If  $m_X$  is not much greater than the momentum transfer in this reaction, one needs to use the  $\bar{\nu}_e e^- \rightarrow \bar{\nu} e^-$  counterparts of Eqs. (A1)-(A5) in evaluating the cross sections.

Additional bounds on the  $X$  couplings to the leptons are available from  $e^+e^- \rightarrow \nu\bar{\nu}\gamma$  scattering, which has been observed at LEP [30-41]. The cross section of this process has been computed in

the literature for the SM [42, 43] as well as its extensions containing extra charged and neutral gauge bosons [44]. In the SM the amplitude at tree level is generated by five diagrams, three of which are mediated by the  $W$  and two by the  $Z$ . The  $X$  contributions are similar in form to the  $Z$  diagrams. Our calculations including the  $X$  contributions agree with the earlier results [43, 44]. The cross section can be written as

$$\sigma_{e\bar{e}\rightarrow\nu\bar{\nu}\gamma} = \frac{1}{2(4\pi)^4 (p_{e^+} + p_{e^-})^2} \int dE_\gamma E_\gamma d(\cos\theta_\gamma) d\bar{\Omega}_\nu \sum_{i,j=e,\mu,\tau} \overline{|\mathcal{M}_{e\bar{e}\rightarrow\nu_i\bar{\nu}_j\gamma}|^2}, \quad (12)$$

where  $E_\gamma$  and  $\theta_\gamma$  are the photon energy and angle with respect to the  $e^+$  or  $e^-$  beam direction in the  $e^+e^-$  center-of-mass frame,  $\bar{\Omega}_\nu$  denotes the solid angle of either  $\nu$  or  $\bar{\nu}$  in the  $\nu\bar{\nu}$  center-of-mass frame, and the formulas for the squared amplitudes are given in Eqs. (A12)-(A14). Our numerical analysis starts in the next section.

### III. CONSTRAINTS FROM $\nu_e e \rightarrow \nu e$

The latest data on the cross section of  $\nu_e e^- \rightarrow \nu e^-$  have been acquired in the E225 experiment at LAMPF [18] and the LSND experiment [19]. They measured the flux-averaged cross-sections  $\bar{\sigma}_{\nu_e e}^{\text{exp}} = (3.18 \pm 0.56) \times 10^{-43} \text{ cm}^2$  and  $\bar{\sigma}_{\nu_e e}^{\text{exp}} = (3.19 \pm 0.48) \times 10^{-43} \text{ cm}^2$ , respectively, corresponding to  $\sigma_{\nu_e e}^{\text{exp}} = (10.0 \pm 1.8) \times 10^{-45} \text{ cm}^2 \bar{E}_\nu / \text{MeV}$  and  $\sigma_{\nu_e e}^{\text{exp}} = (10.1 \pm 1.5) \times 10^{-45} \text{ cm}^2 \bar{E}_\nu / \text{MeV}$  [18, 19] with flux-averaged energy  $\bar{E}_\nu \simeq 31.7 \text{ MeV}$ , the statistical and systematic errors of each having been combined in quadrature. The SM prediction is  $\sigma_{\nu_e e}^{\text{SM}} = 9.3 \times 10^{-45} \text{ cm}^2 \bar{E}_\nu / \text{MeV}$  [19], which translates into  $\bar{\sigma}_{\nu_e e}^{\text{SM}} = 2.95 \times 10^{-43} \text{ cm}^2$ . Performing unconstrained averaging of the two measurements following the Particle Data Group prescription [1] yields  $\bar{\sigma}_{\nu_e e}^{\text{exp}} = (3.19 \pm 0.37) \times 10^{-43} \text{ cm}^2$ , leading to  $\sigma_{\nu_e e}^{\text{exp}} = (10.1 \pm 1.2) \times 10^{-45} \text{ cm}^2 \bar{E}_\nu / \text{MeV}$ .

To explore the constraints on the  $X$  couplings to the leptons from this average value of  $\bar{\sigma}_{\nu_e e}^{\text{exp}}$ , we adopt its 1.64-sigma [90% confidence level (CL)] limits and isolate the  $X$  contribution, including its interference with the SM amplitude, by subtracting out the SM cross-section,  $\bar{\sigma}_{\nu_e e}^{\text{SM}}$ , quoted above. In numerical calculations, we will take  $G_F = 1.166 \times 10^{-5} \text{ GeV}^{-2}$  and  $\sin^2\theta_W = 0.23$ , unless otherwise stated.

We address first the flavor-conserving couplings, turning off the flavor-changing ones in this and the next four sections. Assuming that the coupling products  $L_{ee}$  and  $R_{ee}$  occur at the same time in the  $X$  contribution to the flux-averaged cross-section in Eq. (9), with the squared amplitude given by that in Eq. (A3), we try various values of the  $X$  mass. It turns out that the allowed ranges of the ratios of these parameters to the squared  $X$ -mass become less and less dependent on  $m_X$  fairly quickly if it exceeds  $\sim 40 \text{ MeV}$  and that below this value the effect of the low  $m_X$  on the allowed regions increasingly manifests itself as  $m_X$  decreases. In particular, the restrictions on the ratios grow weaker as the lighter masses get lower. We illustrate all this in Fig. 1 for several examples of  $m_X$  values, where  $\rho_{ee}^{L,R}$  are the ratios normalized by  $2\sqrt{2}G_F$  according to the general definition

$$\rho_{ij}^C = \frac{C_{ij}}{2\sqrt{2}G_F m_X^2}, \quad C_{ij} = g_{\nu_i \nu_j} g_{Ce}, \quad C = L, R. \quad (13)$$

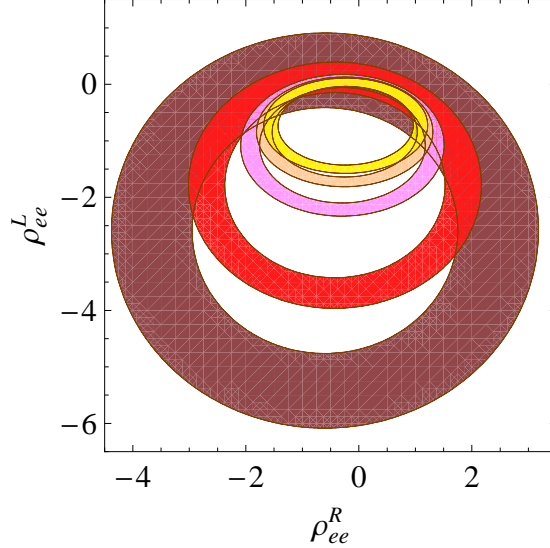


FIG. 1: Values of  $\rho_{ee}^L$  and  $\rho_{ee}^R$  subject to constraints from LAMPF and LSND data on  $\nu_e e \rightarrow \nu e$  scattering for, from largest to smallest rings,  $m_X = 1, 2, 5, 10, 50$  MeV. The yellow (most lightly-shaded) ring, for  $m_X = 50$  MeV, is virtually identical to that for any other  $m_X > 40$  MeV.

It is worth noting that, since in this reaction the magnitude of the momentum exchange in the  $X$  diagram is less than  $|t|_{\max}^{1/2} \simeq (2E_\nu^{\max} m_e)^{1/2} \simeq 7.4$  MeV, the application of the approximate formula in Eq. (8) for  $m_X < 40$  MeV would entail errors of more than  $|t|_{\max}/m_X^2 \sim 3\%$ .

#### IV. CONSTRAINTS FROM $\bar{\nu}_e e \rightarrow \bar{\nu} e$

The cross section of  $\bar{\nu}_e e^- \rightarrow \bar{\nu} e^-$  has been evaluated in several experiments at nuclear power plants. The data on its flux-averaged value  $\bar{\sigma} = \bar{\sigma}_{\bar{\nu}_e e}^{\text{exp}}$  or the corresponding event rate  $R$ , along with their ranges of the final electron's kinetic energy  $T$ , are listed in Table I.<sup>1</sup> To extract the  $X$  couplings permitted by these data, we adopt again the 90%-CL ranges of the experimental

TABLE I: Experimental results on  $\bar{\nu}_e e^- \rightarrow \bar{\nu} e^-$  scattering cross section  $\bar{\sigma}$  or event rate  $R$ .

| Experiment          | $T$ (MeV)   | Measurement  |
|---------------------|-------------|--|
| Savannah River [20] | 1.5-3.0     | $\bar{\sigma} = (0.87 \pm 0.25)\bar{\sigma}_{V-A}$                           |
|                     | 3.0-4.5     | $\bar{\sigma} = (1.70 \pm 0.44)\bar{\sigma}_{V-A}$                           |
| Krasnoyarsk [21]    | 3.150-5.175 | $\bar{\sigma} = (4.5 \pm 2.4) \times 10^{-46} \text{ cm}^2/\text{fission}$   |
| Rovno [22]          | 0.6-2.0     | $\bar{\sigma} = (1.26 \pm 0.62) \times 10^{-44} \text{ cm}^2/\text{fission}$ |
| MUNU [23]           | 0.7-2.0     | $R = (1.05 \pm 0.35)R_{\text{SM}}$   |
| Texono [24]         | 3.0-8.0     | $R = (1.08 \pm 0.26)R_{\text{SM}}$   |

<sup>1</sup> In the Savannah River entries,  $\bar{\sigma}_{V-A}$  is the corresponding cross section in the SM from the  $W$ -mediated diagram alone. The MUNU number for  $R/R_{\text{SM}}$  has been obtained from the observed  $R = 1.07 \pm 0.34$  counts/day and expected  $R_{\text{SM}} = 1.02 \pm 0.10$  counts/day [23].

numbers and subtract out from Eq. (10) the pure SM part given by the usual approximation [28]

$$\frac{d\sigma_{\bar{\nu}_e e}^{\text{SM}}}{dT} = \frac{2G_{\text{F}}^2 m_e}{\pi} \left[ (1 + \bar{g}_L)^2 \left(1 - \frac{T}{E_{\bar{\nu}}}\right)^2 + \bar{g}_R^2 - (1 + \bar{g}_L)\bar{g}_R \frac{m_e T}{E_{\bar{\nu}}^2} \right] \quad (14)$$

appropriate in the  $s \ll m_W^2$  case. For the antineutrino spectrum in Eq. (11), the relevant isotopes are  $k = {}^{235}\text{U}, {}^{238}\text{U}, {}^{239}\text{Pu}, {}^{241}\text{Pu}$ , their relative contributions are taken to be the typical average (over an annual reactor cycle) values  $a_k = 0.54, 0.07, 0.33, 0.06$  [23, 27], respectively, and we employ the  $S_k(E_{\bar{\nu}})$  parametrization provided in Ref. [45].

With the two flavor-conserving parameters,  $L_{ee}$  and  $R_{ee}$ , being present simultaneously as before, we scan the parameter space to observe that the low-mass effect of  $X$  on the allowed regions of its (squared) coupling-to-mass ratios begins to appear strikingly as  $m_X$  goes below  $\sim 25$  MeV and that the bounds tend to become weaker as the mass gets lower, similar to the  $\nu_e e$  case. This pattern is depicted in Fig. 2(a) with some illustrative values of  $m_X$ . Since in this reaction the momentum exchange basically has a size of less than  $s_{\text{max}}^{1/2} = (2E_{\bar{\nu}}^{\text{max}} m_e + m_e^2)^{1/2} \simeq 3.2$  MeV, the use of the approximate formula of the  $\bar{\nu}_e e$  counterpart of Eq. (6) for  $m_X < 25$  MeV would expectedly generate errors of more than  $s_{\text{max}}/m_X^2 \sim 2\%$ .

We can now combine the constraints from the  $\nu_e e \rightarrow \nu e$  and  $\bar{\nu}_e e \rightarrow \bar{\nu} e$  measurements above. We show the overlap areas satisfying the two sets of data in Fig. 2(b). It is clear that the joint constraints reduce the  $\rho_{ee}^{L,R}$  ranges significantly. In this graph, their extreme values specifically are  $(\rho_{ee,\text{min}}^L, \rho_{ee,\text{max}}^L) = (-0.62, 0.65), (-0.22, 0.39), (-0.09, 0.17), (-1.79, 0.12), (-1.57, 0.11)$  and  $(\rho_{ee,\text{min}}^R, \rho_{ee,\text{max}}^R) = (-0.31, 0.41), (-0.81, 0.16), (-0.56, 0.09), (-0.55, 0.08), (-0.54, 0.08)$  for  $m_X = 1, 2, 5, 10, 50$  MeV, respectively, corresponding to the upper limits of  $|L_{ee}|^{1/2}$  and  $|R_{ee}|^{1/2}$

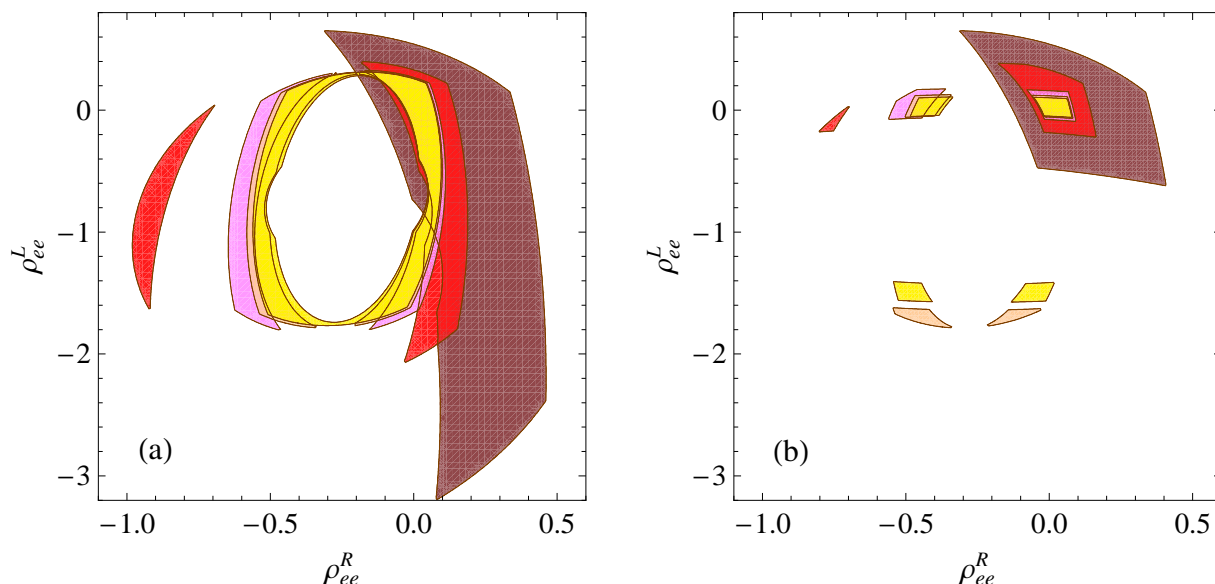


FIG. 2: (a) Values of  $\rho_{ee}^{L,R}$  subject to constraints from  $\bar{\nu}_e e \rightarrow \bar{\nu} e$  data for  $m_X = 1$  MeV (brown, darkest colored), 2 MeV (red), 5 MeV (magenta), 10 MeV (orange), 50 MeV (yellow, most lightly-shaded). The (yellow) area for  $m_X = 50$  MeV is virtually identical to that for any other  $m_X > 25$  MeV. (b) Overlaps between the allowed regions in (a) and Fig. 1.



varying roughly from  $4 \times 10^{-6}$  to  $4 \times 10^{-4}$ . If instead  $m_X = 1, 5, 100$  GeV, the largest limits would be  $\sim 0.007, 0.04, 0.7$ , respectively, from the yellow (most lightly-shaded) areas. Thus, although the low- $m_X$  effect on the allowed  $\rho_{ee}^{L,R}$  areas seen in the earlier figures more or less persists here, the products of  $X$  couplings to the electron neutrino and electron still undergo increasing restraints from these data as  $m_X$  decreases. We should mention that the yellow (most lightly-shaded) regions in Fig. 2(b) for  $m_X \geq 50$  MeV are comparable to their counterparts resulting from the model-independent analyses in Refs. [3, 4] on nonstandard neutrino-electron interactions due to new physics above the electroweak scale.

To paint a more complete picture about how the couplings are constrained by these (anti)neutrino-electron scattering data, we present in Fig. 3(a,b) the upper limits on  $|L_{ee}|^{1/2}$  and  $|R_{ee}|^{1/2}$  following from the allowed extreme values of  $\pm L_{ee}$  and  $\pm R_{ee}$ , respectively, over the  $m_X$  range of interest, assuming in each case that the other coupling product is zero. It is straightforward to see that the solid and dashed curves encompass the  $|L_{ee}|^{1/2}$  or  $|R_{ee}|^{1/2}$  limits implied by the examples in Fig. 2(b). The curves are also roughly compatible with the quoted numbers above for these quantities. In Fig. 3(c,d), we display alternatively the bounds on the vector and

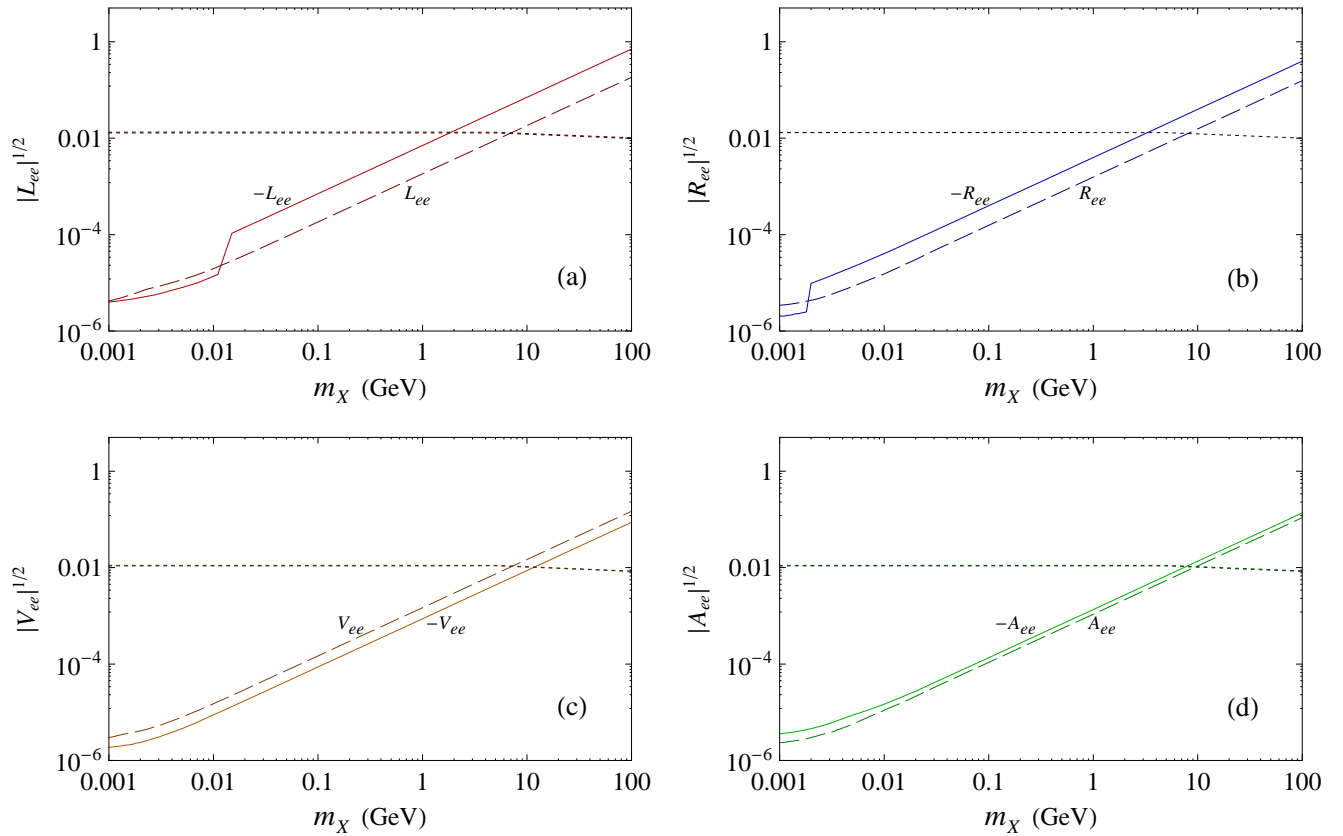


FIG. 3: Upper limits on (a)  $|L_{ee}|^{1/2}$  and (b)  $|R_{ee}|^{1/2}$  versus  $X$  mass from the extreme values of  $\pm L_{ee}$  and  $\pm R_{ee}$ , respectively, allowed by  $\nu_e e \rightarrow \nu_e e$  and  $\bar{\nu}_e e \rightarrow \bar{\nu}_e e$  data only (solid and dashed curves) or  $e^+ e^- \rightarrow \bar{\nu} \nu \gamma$  data only (dotted curves), under the assumption that the other coupling product is zero. Also plotted are the corresponding limits for (c)  $V_{ee} = \frac{1}{2}(L_{ee} + R_{ee})$  and (d)  $A_{ee} = \frac{1}{2}(L_{ee} - R_{ee})$  if only one of these combinations is nonvanishing.

axial-vector combinations  $V_{ee} = \frac{1}{2}(L_{ee} + R_{ee})$  and  $A_{ee} = \frac{1}{2}(L_{ee} - R_{ee})$ , respectively, extracted under the assumption again that only one of them is nonzero. All these special cases demonstrate that, as remarked in the last paragraph, the restrictions become weaker as  $m_X$  gets larger. This is unlike the behavior of the limits from  $e^+e^- \rightarrow \nu\bar{\nu}\gamma$  measurements, which are represented by the dotted curves and will be discussed in Section VI.

## V. CONSTRAINTS FROM $\nu_\mu e \rightarrow \nu e$

The scattering of a muon (anti)neutrino off an electron can probe the  $X$  interactions with them. The most precise experiment on  $\nu_\mu e^- \rightarrow \nu e^-$  and  $\bar{\nu}_\mu e^- \rightarrow \bar{\nu} e^-$  was carried out by the CHARM-II Collaboration. Their low-energy measurement [26], based on the differential cross-section

$$\frac{d\sigma_{\nu_\mu e}}{dy} = \frac{G_F^2 E_\nu m_e}{2\pi} [(g_V + g_A)^2 + (g_V - g_A)^2 (1 - y)^2], \quad (15)$$

where  $y = T/E_\nu$ , and a similar expression for  $\bar{\nu}_\mu e^- \rightarrow \bar{\nu} e^-$  with  $g_A$  replaced by  $-g_A$ , can be translated into

$$(g_V^{\text{exp}} + g_A^{\text{exp}})^2 = 0.289 \pm 0.026, \quad (g_V^{\text{exp}} - g_A^{\text{exp}})^2 = 0.219 \pm 0.023. \quad (16)$$

Comparing these cross-sections with the corresponding ones in Sec. II and assuming that  $g_{V,A}^{\text{exp}}$  consist of SM and  $X$  terms, one can place bounds on (the products of) the  $X$  couplings to the muon (anti)neutrino and electron, depending on the  $X$  mass. Adopting the 90%-CL ranges of the numbers in Eq. (16) and setting the flavor-changing couplings to zero, we obtain the allowed (green) regions of  $\rho_{\mu\mu}^L$  and  $\rho_{\mu\mu}^R$  in Fig. 4 for transfer momenta small compared to  $m_X$ . These results are comparable to their counterparts in the model-independent study of Ref. [3] on neutrino NSI due to new physics above the electroweak scale.

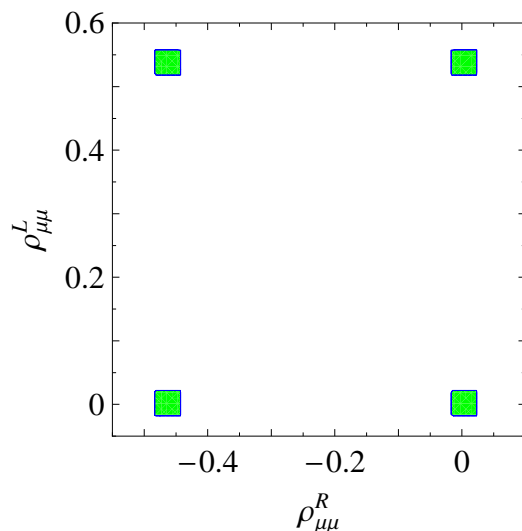


FIG. 4: Values of  $\rho_{\mu\mu}^{L,R}$  allowed by CHARM-II data on  $\nu_\mu e \rightarrow \nu e$  and  $\bar{\nu}_\mu e \rightarrow \bar{\nu} e$  scattering for  $m_X \gtrsim 1$  GeV.

For lower values of  $m_X$ , we are unable to derive bounds on these  $\rho$  parameters due to lack of the relevant information on the (anti)neutrino spectrum and the flux-averaged cross-sections, unlike the  $\nu_e e$  and  $\bar{\nu}_e e$  cases. Nevertheless, based on the findings of the preceding two sections, we can still draw the following conclusion. Since in the CHARM-II experiment  $T = 3\text{--}24\text{ GeV}$  [26] leading to the momentum exchange  $|t|^{1/2} \leq (2m_e T_{\text{max}})^{1/2} \simeq 0.16\text{ GeV}$ , the green (shaded) areas in Fig. 4 can be expected to be valid for  $m_X \gtrsim 1\text{ GeV}$  with errors below  $\sim 2\%$ . We can then infer that  $|L_{\mu\mu}|_{\text{max}}^{1/2} \sim |R_{\mu\mu}|_{\text{max}}^{1/2} \gtrsim 0.004$  as  $m_X$  goes above  $1\text{ GeV}$ .

## VI. CONSTRAINTS FROM $e^+e^- \rightarrow \nu\bar{\nu}\gamma$

The latest measurements of the  $e^+e^- \rightarrow \nu\bar{\nu}\gamma$  cross-section were performed by the ALEPH, DELPHI, L3, and OPAL Collaborations at LEP [30–41] for various center-of-mass energies,  $\hat{s}^{1/2}$ , from about 130 to 207 GeV. The acquired data along with the corresponding SM expectations are listed in Table II. They allow us to impose the constraint  $|\hat{\sigma}_{\text{exp}} - \hat{\sigma}_{\text{SM}} - \sigma_{e\bar{e} \rightarrow \nu\bar{\nu}\gamma}^X| \leq (\delta\sigma_{\text{exp}}^2 + \delta\sigma_{\text{SM}}^2)^{1/2}$ , where  $\hat{\sigma}_{\text{exp,SM}}$  and  $\delta\sigma_{\text{exp,SM}}$  are, respectively, the central values and 90%-CL uncertainties of the  $\sigma_{\text{exp,SM}}$  numbers in Table II,<sup>2</sup> and  $\sigma_{e\bar{e} \rightarrow \nu\bar{\nu}\gamma}^X$  is the  $X$  contribution to the cross section including  $X$ -SM interference terms.

With the much larger energies in this process than in the preceding low-energy cases, it can offer access to the  $m_X$  dependence of the constraints on the  $X$  couplings for larger values of  $m_X$  than the latter could. In addition, the (anti)neutrinos now being only in the final state implies that all their flavors can turn up. Thus,  $e^+e^- \rightarrow \nu\bar{\nu}\gamma$  involves all the  $X$  couplings to them, including the one to  $\nu_\tau$ , via  $L_{\tau\tau}$  and  $R_{\tau\tau}$  which do not participate in the low-energy processes.

Since we are interested in applying the LEP data for  $m_X^2 < \hat{s}$ , the total-width  $\Gamma_X$  needs to be taken into account. However, in our model-independent analysis, its value is unknown, as we leave the  $X$  couplings to other SM particles unspecified and also it may have a component arising from decay channels into final states comprising other nonstandard particles. Consequently, we will assume particular values of  $\Gamma_X$  for illustration.

With  $\Gamma_X$  specified, it is important to ensure that the extracted ranges of  $L_{ij}$  and  $R_{ij}$  satisfy the requirement that the sum of  $\Gamma_{X \rightarrow e^+e^-}$  and the rates of all  $X \rightarrow \nu_i\bar{\nu}_j$  modes not exceed  $\Gamma_X$ . It is straightforward to realize that this amounts to demanding<sup>3</sup>

$$\Gamma_{X \rightarrow e^+e^-} \sum_{i,j=e,\mu,\tau} \Gamma_{X \rightarrow \nu_i\bar{\nu}_j} \leq \frac{1}{4} \Gamma_X^2 \quad (17)$$

with

$$\Gamma_{X \rightarrow \nu_i\bar{\nu}_j} \Gamma_{X \rightarrow e^+e^-} = \frac{\sqrt{m_X^2 - 4m_e^2}}{576\pi^2 m_X} \left[ (|L_{ij}|^2 + |R_{ij}|^2) (m_X^2 - m_e^2) + 6 L_{ij} R_{ji} m_e^2 \right]. \quad (18)$$

<sup>2</sup> The 90%-CL ranges of  $\sigma_{\text{exp,SM}}$  in each one of the entries in this table overlap, except for two in which the overlaps can occur at  $2\sigma$ . Assuming this to be due to statistical flukes, we use  $2\sigma$  uncertainties for these two entries.

<sup>3</sup> With  $\varepsilon$  and  $v$  representing, respectively, the two factors on the left-hand side of Eq. (17), we can always write  $4\varepsilon v \leq (\varepsilon + v)^2 \leq \Gamma_X^2$ .

For consistency, the value of  $\Gamma_X$  picked in each instance needs to be sufficiently large so that the constraints on  $L_{ij}$  and  $R_{ij}$  resulting from the application of this condition are never stricter than the corresponding constraints imposed by the  $e^+e^- \rightarrow \nu\bar{\nu}\gamma$  data.

Based on our numerical exploration, we observe in general that for a fixed  $m_X$  the smaller the appropriately chosen value of  $\Gamma_X$  is, the stronger the bounds from  $e^+e^- \rightarrow \nu\bar{\nu}\gamma$  on the  $X$  couplings, in accord with the expectation that the partial rates which make up  $\Gamma_X$  rise and fall with the couplings. This is illustrated with the blue (shaded) areas in Fig. 5 for some values of  $m_X$  and different  $\Gamma_X$  choices under the assumption that only  $\rho_{ee}^{L,R}$  are nonzero. For these examples, from the top (bottom) plots we extract  $|L_{ee}|_{\max}^{1/2} \simeq |R_{ee}|_{\max}^{1/2} \simeq 0.013, 0.013, 0.010$  (0.016, 0.016, 0.012) corresponding to  $m_X = 0.01, 5, 100$  GeV, respectively. Assuming instead that only  $\rho_{\mu\mu}^{L,R}$  or  $\rho_{\tau\tau}^{L,R}$  are present, we obtain results similar to those for  $\rho_{ee}^{L,R}$ , the difference being due to small interference in the  $ee$  case between the  $X$ - and  $W$ -mediated contributions. These graphs also indicate that as  $m_X$  increases the constraints on  $\rho_{ee}^{L,R}$ ,  $\rho_{\mu\mu}^{L,R}$ , or  $\rho_{\tau\tau}^{L,R}$  tend to get stronger provided that  $\Gamma_X/m_X$  does not change appreciably.

Moreover, comparing the  $\rho_{ee,\mu\mu}^{L,R}$  plots with Figs. 2(b) and 4, respectively, we notice that for  $m_X$  values of a few GeV or higher the areas permitted by the (anti)neutrino-electron scattering data can significantly shrink to those around the origin after the inclusion of the  $e^+e^- \rightarrow \nu\bar{\nu}\gamma$

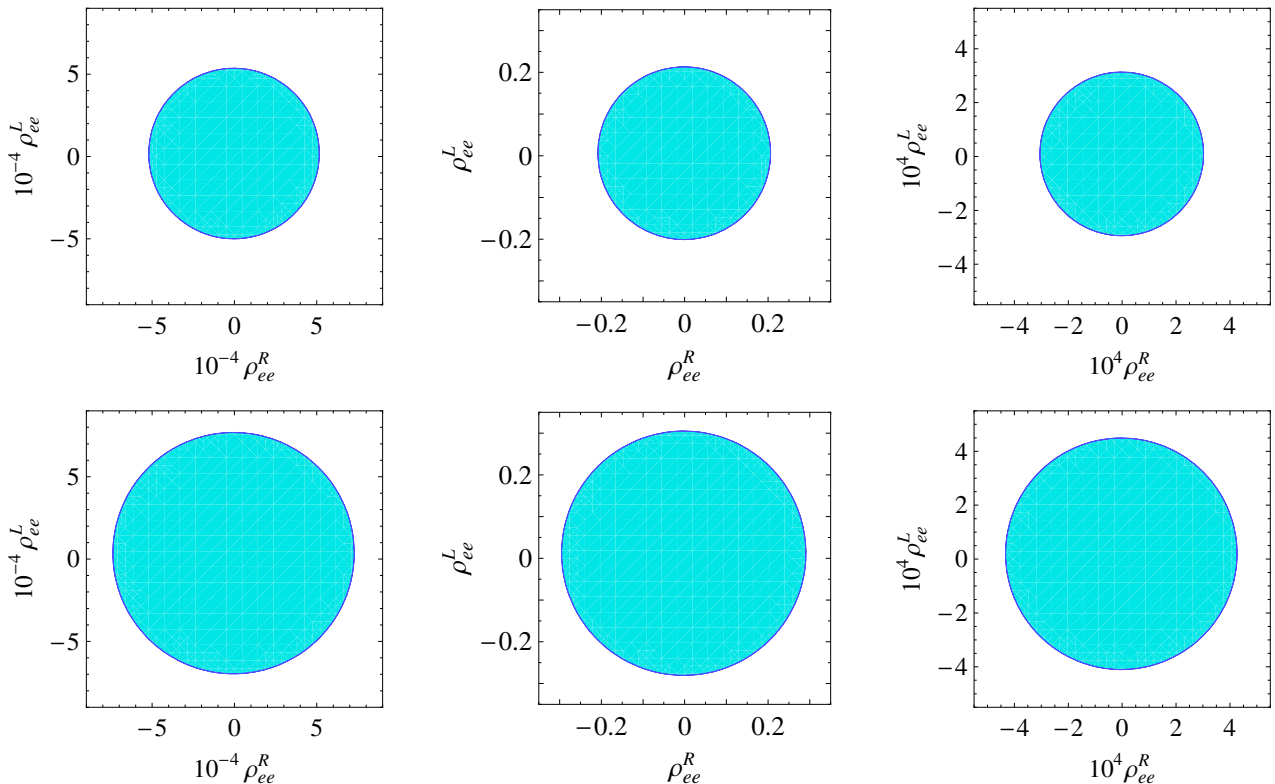


FIG. 5: Top plots: values of  $\rho_{ee}^L$  and  $\rho_{ee}^R$  (blue areas) allowed by LEP data on  $e^+e^- \rightarrow \nu\bar{\nu}\gamma$  and the  $\Gamma_X$  requirement in Eq. (17) for, from left to right,  $m_X = 0.01, 5, 100$  GeV and  $\Gamma_X = 0.05, 25, 300$  keV, respectively, in the limit that all the other  $\rho_{ij}^{L,R}$  vanish. Bottom plots: same as top ones, but for  $\Gamma_X$  being twice as large.

constraints, depending on  $\Gamma_X$ , and increasingly so as  $m_X$  goes up. Thus, the two sets of data offer complementary restrictions on these  $\rho$  parameters, with the former (latter) yielding stronger constraints for lower (higher) masses. Such complementarity is also visible in the limits on  $L_{ee}$  and  $R_{ee}$ , or their combinations, in the special cases depicted in Fig. 3, where the dotted curves represent the limits from  $e^+e^- \rightarrow \nu\bar{\nu}\gamma$ . These dotted curves correspond to the  $\Gamma_X$  choices, as in the top plots of Fig. 5, which are roughly the smallest ones satisfying the consistency requirement mentioned after Eq. (17).

Before moving on, we note that in the family-universal limit,  $\rho_{ee}^C = \rho_{\mu\mu}^C = \rho_{\tau\tau}^C$ , of the neutrino sector, the allowed ranges of these ratios are somewhat smaller than in the family-nonuniversal case due to the decrease in the number of free parameters. In a specific model, the reduction of the  $X$ -coupling ranges is also generally expected to happen because the model parameters are related to each other and subject to various data (see, *e.g.*, Refs. [6, 10]).

Another situation in which the constraints on the  $X$  couplings can be stronger is when  $X$  mixes with the SM gauge bosons. In such a case, the mixing usually leads to a substantial increase in the number of experimental observables that need to be taken into account with the mixing angle being the only additional free parameter, and as a consequence the  $X$  couplings become more restrained.<sup>4</sup> Thus, the numerical results of our analysis correspond to those in the limit that the mixing is negligible.

## VII. CONSTRAINTS ON SEPARATE FLAVOR-CONSERVING COUPLINGS

There are observables that can yield bounds on the  $X$  couplings to the electron,  $g_{Le,Re}$ , and neutrinos,  $g_{\nu_i\nu_i}$ , separately. The resulting limits will then complement the limits on the products of the couplings determined in the earlier sections. To evaluate the most important constraints, we look at those from  $e^+e^-$  scattering data at the  $Z$ -pole and the measured anomalous magnetic moment of the electron, as well as searches for a nonstandard spin-1 particle at fixed-target and beam-dump experiments.

The  $Z$ -pole observables with sensitivity to  $g_{Le,Re}$  are the rate  $\Gamma_{Z \rightarrow e^+e^-} \simeq |\overline{\mathcal{M}}_{Z \rightarrow \bar{e}e}|^2 / (16\pi m_Z)$  and the parameter  $A_e = (|L'_e|^2 - |R'_e|^2) / (|L'_e|^2 + |R'_e|^2)$  associated with the forward-backward asymmetry, which follow from the amplitude  $\mathcal{M}_{Z \rightarrow \bar{e}e} = \bar{e} \not{\epsilon}_Z (L'_e P_L + R'_e P_R) e$ . The presence of  $X$  causes modifications to the  $Ze^+e^-$  vertex and electron self-energy diagrams at the one-loop level. Calculating the  $X$  contributions and combining them with the SM ones, we have

$$C'_e = \frac{g \bar{g}_C}{c_w} (1 + \mathcal{F}(\delta) g_{Ce}^2), \quad C = L, R, \quad \delta = \frac{m_X^2}{m_Z^2},$$

$$\mathcal{F}(\delta) = \frac{1}{16\pi^2} \left\{ -\frac{7}{2} - 2\delta - (3 + 2\delta) \ln \delta - 2(1 + \delta)^2 \left[ \ln \delta \ln \frac{\delta}{1 + \delta} + \text{Li}_2 \left( -\frac{1}{\delta} \right) \right] \right. \\ \left. - i\pi \left[ 3 + 2\delta + 2(1 + \delta)^2 \ln \frac{\delta}{1 + \delta} \right] \right\}, \quad (19)$$

where  $\bar{g}_{L,R}$  are defined in Eq. (3) and  $\text{Li}_2$  is the dilogarithm. The expression for the real part

<sup>4</sup> This can occur in scenarios involving an extra U(1) gauge boson, such as considered in Refs. [46, 47].

of  $\mathcal{F}$  has been derived previously [48]. To probe  $g_{\nu_i\nu_i}$ , the relevant observable is  $\Gamma_{Z\rightarrow\nu\bar{\nu}}$ , which dominates  $\Gamma_{Z\rightarrow\text{invisible}}$  and comes from an amplitude analogous to that in  $Z \rightarrow e^+e^-$ , but without the right-handed coupling. Since the neutrinos are not observed,

$$\Gamma_{Z\rightarrow\nu\bar{\nu}} = \sum_{i=e,\mu,\tau} \Gamma_{Z\rightarrow\nu_i\bar{\nu}_i} = \frac{g^2 m_Z}{96\pi c_W^2} \sum_{i=e,\mu,\tau} |1 + \mathcal{F}(\delta) g_{\nu_i\nu_i}^2|^2. \quad (20)$$

Now, the SM predicts that [8]  $\Gamma_{Z\rightarrow e^+e^-}^{\text{sm}} = 84.01 \pm 0.07$  MeV,  $A_e^{\text{sm}} = 0.1475 \pm 0.0010$ , and  $\Gamma_{Z\rightarrow\text{invisible}}^{\text{sm}} = 501.69 \pm 0.06$  MeV, whereas experiments yield [1]  $\Gamma_{Z\rightarrow e^+e^-}^{\text{exp}} = 83.91 \pm 0.12$  MeV,  $A_e^{\text{exp}} = 0.1515 \pm 0.0019$ , and  $\Gamma_{Z\rightarrow\text{invisible}}^{\text{exp}} = 499.0 \pm 1.5$  MeV. Accordingly, to restrain the  $X$  couplings we can require them to satisfy the 90% CL ranges<sup>5</sup>  $83.71 \text{ MeV} \leq \Gamma_{Z\rightarrow e^+e^-} \leq 84.11 \text{ MeV}$ ,  $0.1459 \leq A_e \leq 0.1546$ , and  $497 \text{ MeV} \leq \Gamma_{Z\rightarrow\nu\bar{\nu}} \leq 502 \text{ MeV}$ . In extracting the couplings from these  $Z$ -pole measurements, for the SM parts we employ the tree-level formulas along with the effective values  $g_{\text{eff}} = 0.6517$  and  $s_{\text{w,eff}}^2 = 0.23146$  which lead to the  $\Gamma_{Z\rightarrow e^+e^-}^{\text{sm}}$  and  $A_e^{\text{sm}}$  numbers above within their errors and  $\Gamma_{Z\rightarrow\nu\bar{\nu}}^{\text{sm}} = 501.26 \text{ MeV} < \Gamma_{Z\rightarrow\text{invisible}}^{\text{sm}}$  in accord with expectation. We show the results in Fig. 6 for  $g_{Le,Re}$ ,  $g_{\nu_i\nu_i}$ , and the combinations  $g_{Ve,Ae} = \frac{1}{2}(g_{Le} \pm g_{Re})$  for the special cases in which only one of them is nonzero (the dotted curves). In Fig. 6(b) the  $g_{Ve,Ae}$  (dotted) curves coincide, which can be understood from the form of  $C_e$  in Eq. (19).

The anomalous magnetic moment of the electron,  $a_e = g_e/2 - 1$ , has been measured very precisely and therefore provides additional important constraints on  $g_{Le,Re}$  or  $g_{Ve,Ae}$ . In terms of

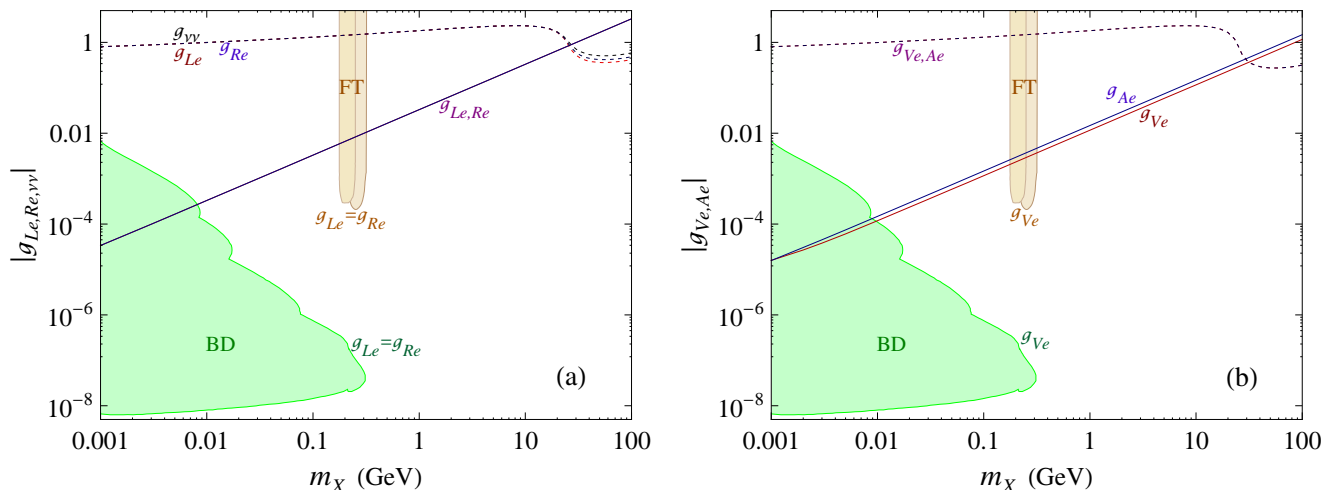


FIG. 6: The dotted curves describe the upper limits on (a)  $|g_{Le,Re,\nu_i}|$  and (b)  $|g_{Ve,Ae}|$  from  $Z$ -pole data under the assumption that only one of the couplings is nonzero in each case, while the solid curves describe the corresponding limits from the measured  $g_e - 2$ . The light-orange and light-green regions contain values of (a)  $g_{Le} = g_{Re}$  and (b)  $g_{Ve}$  disallowed by electron-nucleus fixed-target scattering (FT) and electron beam-dump (BD) experiments under the assumption that  $g_{Ae} = 0$  and the branching ratio  $\mathcal{B}(X \rightarrow e^+e^-) = 1$ .

<sup>5</sup> We have taken the lower (upper) bound of  $A_e$  ( $\Gamma_{Z\rightarrow\nu\bar{\nu}}$ ) to be its SM lower (upper) value because  $A_e^{\text{exp}}$  is above  $A_e^{\text{sm}}$  ( $\Gamma_{Z\rightarrow\text{invisible}}^{\text{exp}}$  is below  $\Gamma_{Z\rightarrow\text{invisible}}^{\text{sm}}$ ) by  $\sim 2$  sigmas.

the latter, the  $X$  contribution is [49]

$$a_e^X = \frac{m_e^2}{4\pi^2 m_X^2} (g_{V_e}^2 f_V(r) + g_{A_e}^2 f_A(r)) , \quad (21)$$

where  $r = m_e^2/m_X^2$ ,

$$f_V(r) = \int_0^1 dx \frac{x^2 - x^3}{1 - x + rx^2} , \quad f_A(r) = \int_0^1 dx \frac{-4x + 5x^2 - x^3 - 2rx^3}{1 - x + rx^2} . \quad (22)$$

The SM prediction for  $a_e$  is compatible with its latest measurement, the difference between the two being  $a_e^{\text{exp}} - a_e^{\text{SM}} = (-105 \pm 82) \times 10^{-14}$  [50]. Consequently, for the  $X$  contribution we can impose the 90% CL range  $-2.4 \times 10^{-12} \leq a_e^X \leq 0.3 \times 10^{-12}$ . This translates into the limits (solid curves) graphed in Fig. 6. Evidently, these results are stricter (weaker) than those in the previous paragraph for  $m_X$  below (above)  $\sim 30$  GeV.

There are also restrictions on  $g_{V_e}$  from the recent electron-nucleus fixed-target scattering experiments by the A1 and APEX Collaborations [51], but so far only for  $m_X = 175$ -300 MeV. However, the strictness of the constraints depends on the assumed interactions of  $X$  with other particles. Since the A1 and APEX analyses presupposed that  $X$  coupled mainly to the electromagnetic current (and hence had negligible axial-vector couplings to fermions), following Ref. [52], their limits on  $g_{V_e}$  apply most strongly to the case in which the channel  $X \rightarrow e^+e^-$  highly dominates the  $X$  decay. In the limiting case that the branching ratio  $\mathcal{B}(X \rightarrow e^+e^-) = 1$ , the excluded zone is displayed as the light-orange patch in Fig. 6(b)<sup>6</sup> and the corresponding one in Fig. 6(a), where for the latter we have employed the fact that a limit on  $g_{V_e}$  in the absence of  $g_{A_e} = \frac{1}{2}(g_{L_e} - g_{R_e})$ , as assumed by A1 and APEX in interpreting their measurements [51], implies a limit on  $g_{L_e} = g_{R_e}$ . For  $X \rightarrow e^+e^-$  not being the dominant decay mode,  $\mathcal{B}(X \rightarrow e^+e^-) < 1$ , such as in a complete study considering the  $X$  couplings to all fermions, the restraints would be lessened and the light-orange regions move upward by a factor of  $[\mathcal{B}(X \rightarrow e^+e^-)]^{-1/2}$ .

For  $m_X$  under a few hundred MeV, further constraints might be available from electron beam-dump experiments, where  $X$  could be produced by bremsstrahlung from an electron scattering off a nuclear target and pass through a shield before decaying into an  $e^+e^-$  pair in front of the detector [52–54]. The  $X$  decay length  $l_X$  would then need to be between the length of the target plus the shield and the total distance from the target to the detector. In view of the latest information on the relevant past experiments collected in Ref. [53], including their electron beam energies and shield lengths, one might ask if their data could bound the  $X$  couplings. Since  $l_X = p_X/(\Gamma_X m_X)$ , with  $p_X$  being the laboratory momentum of  $X$ , the answer would depend on the choice of  $\Gamma_X$  or the assumed interactions of  $X$ , as in the last paragraph. For instance, if  $\Gamma_X$  has the values chosen for the dotted curves in Fig. 3, we determine that the electron beam-dump

<sup>6</sup> Since the A1 and APEX bounds presupposed that  $X$  coupled only to the electromagnetic current [51, 52], for the mass range  $2m_\mu < m_X \leq 300$  MeV, before drawing the light-orange patch, we have lowered them by a factor of  $\mathcal{S} = [1 + \Gamma_{X \rightarrow \mu^+\mu^-} (1 + R(m_X))/\Gamma_{X \rightarrow e^+e^-}]^{1/2}$  in order to account for the opening of the  $\mu^+\mu^-$  and  $\pi^+\pi^-$  decay channels of  $X$ . Here  $R$  is the energy-dependent ratio  $\sigma(e^+e^- \rightarrow \text{hadrons})/\sigma(e^+e^- \rightarrow \mu^+\mu^-)$  available from Ref. [1] and the rate [53]  $\Gamma_{X \rightarrow l+l^-} = g_V^2 m_X (1 + 2m_l^2/m_X^2) (1 - 4m_l^2/m_X^2)^{1/2}/(12\pi)$  for  $l = e, \mu$  contains the vector coupling bound  $g_V$  supplied by A1 and APEX [51].

experiments listed in Ref. [53] could not probe  $X$  because it would decay well inside their shields. On the other hand, if  $\Gamma_X$  is smaller and within the appropriate range, it would be possible for  $X$  to decay in the detection region depending on  $m_X$ . In that case, we can look at the latest limits supplied in Ref. [53] whose authors also assumed that  $X$  effectively coupled only to the electromagnetic current and thus had vanishing axial-vector couplings. For  $\mathcal{B}(X \rightarrow e^+e^-) = 1$ , their results translate into the disfavored parameter space represented by the light-green portions of Fig. 6,<sup>7</sup> while for  $X \rightarrow e^+e^-$  not being dominant the restrictions would decrease and the light-green zones would shift upward also by a factor of  $[\mathcal{B}(X \rightarrow e^+e^-)]^{-1/2}$ .

Some additional constraints may come from the measurements of  $e^+e^- \rightarrow e^+e^-l^+l^-$  scattering for  $l = e, \mu, \tau$ , but the available data, collected at energies around the  $Z$  resonance by the ALEPH Collaboration [55], are rather limited compared to most of those discussed above. Since the observed numbers of events for the different leptonic final-states were consistent within up to about 40% with the SM expectations [55], to extract the constraints on the  $X$  couplings to the electron we may require that their effects be less than 20% of the SM contributions. To estimate the cross section including the  $X$  contribution, we employ the CalcHEP package [56]. The resulting constraints depend again on the choices of  $\mathcal{B}(X \rightarrow e^+e^-)$ . If  $\mathcal{B}(X \rightarrow e^+e^-) = 1$  and only one of the  $X$  couplings is nonzero at a time, we get  $|g_{Le,Re}|$  below roughly 0.2, 0.08, 0.5 for  $m_X = 0.01, 1, 100$  GeV, respectively. The bounds would be weaker if  $\mathcal{B}(X \rightarrow e^+e^-) < 1$ . Hence they generally are not more stringent than the strictest bounds exhibited in Fig. 6.

The results presented in Figs. 3 and 6 illustrate how the various measurements complement each other in probing the  $X$  couplings. If the electron and neutrino couplings of  $X$  are not very dissimilar in size, the (anti)neutrino-electron scattering and  $e^+e^- \rightarrow \nu\bar{\nu}\gamma$  data can be expected to offer the strictest constraints. If instead one of the electron and neutrino couplings is much larger than the other, then the  $Z$ -pole data and measured  $a_e$  may provide the best constraints, depending on  $m_X$ . For a sub-GeV mass, electron fixed-target and beam-dump experiments can yield the most stringent test in the case of  $X$  dominantly coupling to the electron. Furthermore, if  $m_X$  is a few GeV or lower, future searches of  $e^+e^- \rightarrow \gamma X$ ,  $X \rightarrow e^+e^-$  at high-luminosity colliders may offer competitive probes [16]. We note that the case of the electron couplings being much larger than the neutrino couplings could occur even if  $X$  hails from an extra gauge sector, one example being the dark/hidden photon, which is a spin-1 mass-eigenstate associated with a new U(1) symmetry and coupling predominantly to SM charged fermions through the electromagnetic current [52, 53].

Also, our results are applicable to some of the scenarios mentioned in Section I which may explain certain experimental anomalies. In particular, our bounds on the  $X$  couplings already probe parts of the parameter space of the spin-1 particles that may have been the factors behind the unexpected observations of the 511-keV emission from our galactic bulge and of the positron excess in cosmic rays, but the bounds do not yet test the validity of these scenarios. In the former case,  $X$  has mass of  $\mathcal{O}(1 \text{ MeV})$  and may be detectable with future neutrino telescopes if  $g_{\nu_i\nu_i} \gtrsim 10^{-5}$  [9], which easily satisfies the  $g_{\nu_i\nu_i}$  limit in Fig. 6(a) and implies that  $g_{Le,Re}$  need to be sufficiently small to evade the restrictions depicted in Fig. 3(a). In the latter scenario,  $m_X$  is of order a few GeV and the corresponding limits given in Figs. 3 and 6 indicate the level of

---

<sup>7</sup> For  $m_X > 2m_\mu$ , we have again reduced the bounds from Ref. [53] by the corresponding factor  $\mathcal{S}$ .



constraints on  $g_{L_e, R_e, \nu_i \nu_i}$  from current data, but future searches in the BESIII experiment could be sensitive to  $g_{L_e, R_e}$  and  $g_{\nu_i \nu_i}$  as small as  $10^{-4}$  and  $10^{-5}$ , respectively [11].

## VIII. FLAVOR-CHANGING COUPLINGS

Finally, we explore the bounds on the flavor-changing parameters,  $L_{ij}$  and  $R_{ij}$  for  $i \neq j$ , as well as the corresponding  $\rho$  parameters, from the same experimental inputs as considered in Sections III-VI. To do so, we assume that only one of these ( $L, R$ ) pairs is nonzero at a time and turn off all the flavor-conserving ones,  $L_{ii} = R_{ii} = 0$ . Furthermore, here we slightly modify the definition of  $L_{ij}$  to  $L_{ij} = |g_{\nu_i \nu_j}| g_{L_e} = L_{ji}$  to make it real, and similarly with  $R_{ij}$ .

We display in Fig. 7 the values of  $\rho_{\mu e}^{L, R} = \rho_{e\mu}^{L, R}$  permitted by the  $\nu_e e$  and  $\bar{\nu}_e e$  scattering data and, if  $m_X \gtrsim 1$  GeV, by the  $\nu_\mu e$  and  $\bar{\nu}_\mu e$  scattering data. As Fig. 7(c) indicates, we find that the maximal values  $|\rho_{e\mu}^{L(R)}|_{\max}$  vary from 1.3 to 0.10 (0.70 to 0.11) as  $m_X$  rises from 1 MeV to 1 GeV, and accordingly  $|L_{e\mu}|_{\max}^{1/2}$  ( $|R_{e\mu}|_{\max}^{1/2}$ ) varies from  $7(5) \times 10^{-6}$  to 0.002 (0.002) in this mass range. If  $m_X = 5(100)$  GeV instead, one would find  $|L_{e\mu}|_{\max}^{1/2} \simeq |R_{e\mu}|_{\max}^{1/2} \sim 0.004(0.02)$  from the smallest (green) area. For the  $e\tau$  parameters, the allowed regions are the same as those for  $e\mu$  subject to the  $\nu_e e$  and  $\bar{\nu}_e e$  data. Thus,  $|\rho_{e\tau}^{L(R)}|_{\max}$  changes from 1.3 to 0.40 (0.70 to 0.19) for  $m_X = 1$ -50 MeV, as Fig. 7(c) shows, and the corresponding numbers for  $m_X \gtrsim 40$  MeV are practically the same as those for  $m_X = 50$  MeV. The limits on  $\rho_{\tau\mu, \mu\tau}^{L, R}$  come from  $\nu_\mu e$  and  $\bar{\nu}_\mu e$  scattering, and so  $|\rho_{\mu\tau}^{L, R}|_{\max} \simeq 0.1$  for  $m_X \gtrsim 1$  GeV. It is evident from these examples that the patterns of low- $m_X$  dependence seen in the flavor-conserving cases roughly turn up again here.

In Fig. 8 we present the ranges of  $\rho_{\mu e}^{L, R} = \rho_{e\mu}^{L, R}$  satisfying the  $e^+ e^- \rightarrow \nu \bar{\nu} \gamma$  restrictions (blue shaded areas) for the same  $m_X$  and  $\Gamma_X$  choices as in the top plots in Fig. 5. In drawing Fig. 8, we have taken into account the fact that  $\rho_{\mu e}^{L, R}$  and  $\rho_{e\mu}^{L, R}$  contribute to the cross section via a pair of charge-conjugate final states. For these instances, the boundaries of the blue regions imply

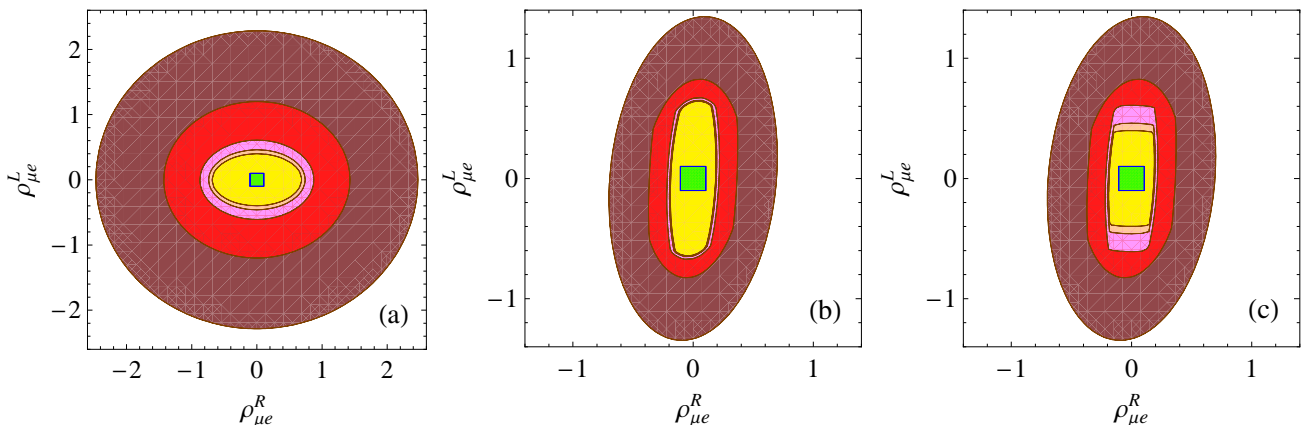


FIG. 7: Values of  $\rho_{\mu e}^L$  and  $\rho_{\mu e}^R$  allowed by (a)  $\nu_{e,\mu} e \rightarrow \nu e$  data, (b)  $\bar{\nu}_{e,\mu} e \rightarrow \bar{\nu} e$  data, and (c) all of them for  $m_X = 1$  MeV (brown, darkest colored), 2 MeV (red), 5 MeV (magenta), 10 MeV (orange), 50 MeV (yellow, most lightly-shaded), and  $m_X \gtrsim 1$  GeV (smallest green areas) in the limit that all the other  $\rho_{ij}^{L, R}$  vanish.

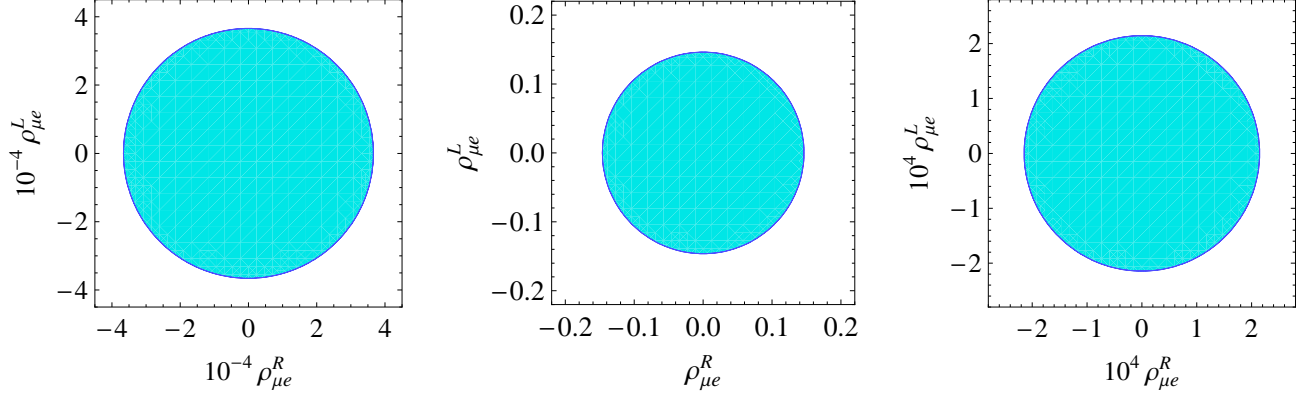


FIG. 8: Values of  $\rho_{\mu e}^{L,R} = \rho_{e\mu}^{L,R}$  allowed by  $e^+e^- \rightarrow \nu\bar{\nu}\gamma$  data and  $\Gamma_X$  requirement in Eq. (17) for, from left to right,  $m_X = 0.01, 5, 100$  GeV and  $\Gamma_X = 0.05, 25, 300$  keV, respectively, if all the other  $\rho_{ij}^{L,R}$  vanish.

$|L_{\mu e}|_{\max}^{1/2} = |R_{\mu e}|_{\max}^{1/2} \simeq 0.011, 0.011, 0.008$  for  $m_X = 0.01, 5, 100$  GeV, respectively. These results are the same as those for the corresponding  $e\tau$  and  $\mu\tau$  parameters.

The examples in the last two paragraphs demonstrate as in Section VI that the  $e^+e^- \rightarrow \nu\bar{\nu}\gamma$  constraints can be stronger than those from  $\nu e$  and  $\bar{\nu}e$  scattering data, depending on  $m_X$  and  $\Gamma_X$ , especially for  $m_X$  above 1 GeV. Hence again the two sets of measurements are complementary to each other in bounding the  $X$  leptonic couplings.

Lastly, we note that these flavor-changing parameters can induce at the one-loop level flavor-violating  $X$ -mediated transitions involving charged leptons, such as  $\mu \rightarrow 3e$  and  $\tau \rightarrow 3e$ . The loop consists of internal  $W$  and flavor-changing neutrino lines, and  $X$  is attached to the neutrino line. Although the experimental upper limits of their branching ratios are very stringent, whether or not they could yield strict bounds on the flavor-changing  $X$  couplings depends on whether the complete model possesses a Glashow-Iliopoulos-Maiani-like mechanism in the lepton sector. If it does, the branching ratios will be very suppressed by the neutrino masses, as in Eq. (A18), allowing the couplings to evade the experimental limits. However, if such a mechanism is absent, the couplings will be highly suppressed compared to the results found above.

## IX. CONCLUSIONS

There has been some regained interest in new light spin-1 particles, with mass in the regime of several GeV to sub-GeV, in the hope of explaining a number of experimental anomalies and unexpected astronomical observations. We have explored in this work the constraints on the neutrino and electron interactions of such a particle from several sets of lepton scattering data. The new boson,  $X$ , is assumed to be electrically and color neutral, without mixing with the standard-model gauge bosons, and its couplings with the leptons are taken to be sufficiently general for a model-independent approach. Our analysis starts with the case of only flavor-conserving couplings. We utilize the  $\nu_e e^- \rightarrow \nu e^-$  scattering data acquired in the E225 experiment at LAMPF and the LSND experiment, in tandem with the  $\bar{\nu}_e e^- \rightarrow \bar{\nu} e^-$  data obtained from several experiments at nuclear power plants, to place bounds on the chiral couplings of  $X$  to the electron neutrino and electron, via the  $\rho_{ee}^{L,R}$  parameters defined in the main text. We illustrate how, for

a relatively light  $X$ , its mass may substantially affect the determination of its couplings to these leptons. Subsequently, constraints on their muon-neutrino counterparts are imposed by means of the CHARM-II data on  $\nu_\mu e^- \rightarrow \nu e^-$  and  $\bar{\nu}_\mu e^- \rightarrow \bar{\nu} e^-$  scattering. The LEP measurements of  $e^+e^- \rightarrow \nu\bar{\nu}\gamma$  are then employed to derive a complementary set of experimental bounds on  $\rho_{ee,\mu\mu}^{L,R}$ , plus the only restraints on  $\rho_{\tau\tau}^{L,R}$ , the result of which shows significant dependence on the mass and decay width of the  $X$  boson. As an important supplement, we also evaluate constraints on the respective flavor-conserving  $X$  couplings to the electron and neutrinos from  $Z$ -pole data, the measured  $g_e - 2$ , and searches at fixed-target and beam-dump experiments. Finally, we apply the same inputs from the (anti)neutrino-electron and  $e^+e^- \rightarrow \nu\bar{\nu}\gamma$  scattering experiments to the case where only one pair of flavor-violating chiral couplings of  $X$  is dominant to find their allowed ranges. In summary, under our assumptions, the current experimental data restrict the couplings within narrow regions consistent with zero over a wide range of the new boson mass.

### Acknowledgments

We would like to thank Sechul Oh for conversations which led to this work. We also thank Takaaki Nomura and Kei Yagyu for assistance with CalcHEP. This work was supported in part by National Center for Theoretical Sciences, the National Science Council of R.O.C. under Grants Nos. NSC-100-2628-M-008-003-MY4, NSC-99-2112-M-008-003-MY3, and NSC-100-2811-M-008-036, and the NCU Plan to Develop First-Class Universities and Top-Level Research Centers.

### Appendix A: Squared amplitudes and $e^+e^- \rightarrow \nu\bar{\nu}\gamma$ data

The tree-level contribution of the SM to the amplitude for  $\nu_i e^- \rightarrow \nu_j e^-$  with  $i = j = e$  arises from  $u$ -channel  $W$ -mediated and  $t$ -channel  $Z$ -mediated diagrams. The  $X$ -mediated diagram contributes in the  $t$ -channel. For  $i = j = \mu$  the  $W$ -mediated contribution is absent, while for  $i \neq j$  only the  $X$  contribution is present. Neglecting the neutrino mass, averaging the absolute square of the amplitude over the initial electron spins, the incident neutrino being left-handed, and summing the amplitude over the final spins, we then arrive at for  $i = e$  or  $\mu$

$$\overline{|\mathcal{M}_{\nu_i e \rightarrow \nu_i e}|^2} = \overline{|\mathcal{M}_{\nu_i e \rightarrow \nu_i e}^{\text{SM}}|^2} + \overline{|\mathcal{M}_{\nu_i e \rightarrow \nu_i e}|_X^2}, \quad (\text{A1})$$

$$\begin{aligned} \overline{|\mathcal{M}_{\nu_i e \rightarrow \nu_i e}^{\text{SM}}|^2} &= \frac{\omega g^4}{2\mathcal{U}_W^2} \left[ (s - m_e^2)^2 + \frac{m_e^4 t}{m_W^2} + \frac{m_e^4 (u - m_e^2)^2}{4m_W^4} \right] \\ &+ \frac{\omega g^4}{c_w^2 \mathcal{U}_W \mathcal{T}_Z} \left\{ \bar{g}_L \left[ (s - m_e^2)^2 + \frac{m_e^4 t}{2m_W^2} \right] + \bar{g}_R m_e^2 \left[ t + \frac{(u - m_e^2)^2}{2m_W^2} \right] \right\} \\ &+ \frac{g^4}{2c_w^4 \mathcal{T}_Z^2} \left[ \bar{g}_L^2 (s - m_e^2)^2 + \bar{g}_R^2 (u - m_e^2)^2 + 2\bar{g}_L \bar{g}_R m_e^2 t \right], \quad (\text{A2}) \end{aligned}$$

$$\begin{aligned}
\overline{|\mathcal{M}_{\nu_i e \rightarrow \nu_j e}|_X^2} &= \frac{2\omega g^2}{\mathcal{U}_W \mathcal{T}_X} \left\{ L_{ee} \left[ (s - m_e^2)^2 + \frac{m_e^4 t}{2m_W^2} \right] + R_{ee} m_e^2 \left[ t + \frac{(u - m_e^2)^2}{2m_W^2} \right] \right\} \\
&+ \frac{2g^2}{c_w^2 \mathcal{T}_Z \mathcal{T}_X} \left\{ \bar{g}_L [L_{ii}(s - m_e^2)^2 + R_{ii} m_e^2 t] + \bar{g}_R [R_{ii}(u - m_e^2)^2 + L_{ii} m_e^2 t] \right\} \\
&+ \frac{2}{\mathcal{T}_X^2} [L_{ii}^2 (s - m_e^2)^2 + R_{ii}^2 (u - m_e^2)^2 + 2L_{ii} R_{ii} m_e^2 t] , \tag{A3}
\end{aligned}$$

$$\begin{aligned}
s &= (p_\nu + p_e)^2 , & t &= (p'_e - p_e)^2 , & u &= 2m_e^2 - s - t , \\
\mathcal{T}_P &= t - m_P^2 , & \mathcal{U}_P &= u - m_P^2 , & \mathbf{C}_{ii} &= g_{\nu_i \nu_i} g_{\mathbf{C}e} , & \mathbf{C} &= L, R , \tag{A4}
\end{aligned}$$

where  $\omega = 1(0)$  if  $i = e(\mu)$ , the expression in Eq.(A3) contains  $X$ -SM interference terms plus a purely  $X$ -induced part, and  $p_\nu$  and  $p_e$  ( $p'_\nu$  and  $p'_e$ ) are the four-momenta of the initial (final) neutrino and electron, respectively. For  $j \neq i$

$$\overline{|\mathcal{M}_{\nu_i e \rightarrow \nu_j e}|^2} = \frac{2}{\mathcal{T}_X^2} [ |L_{ji}|^2 (s - m_e^2)^2 + |R_{ji}|^2 (u - m_e^2)^2 + 2L_{ij} R_{ji} m_e^2 t ] , \quad \mathbf{C}_{ij} = g_{\nu_i \nu_j} g_{\mathbf{C}e} , \tag{A5}$$

where we have used  $\text{Re}(L_{ji}^* R_{ji}) = L_{ij} R_{ji}$  following from  $g_{\nu_i \nu_i}^* = g_{\nu_i \nu_i}$ . In the laboratory frame where the initial electron is at rest,

$$s = 2E_\nu m_e + m_e^2 , \quad t = -2m_e T , \tag{A6}$$

where  $E_\nu$  is the energy of the incident neutrino and  $T$  the kinetic energy of the recoiling electron. From the scattering kinematics, it is simple to show [57]

$$0 \leq T \leq \frac{2E_\nu^2}{2E_\nu + m_e} . \tag{A7}$$

For the  $\bar{\nu}_i e^- \rightarrow \bar{\nu}_j e^-$  scattering with  $i = j = e$ , the amplitude receives contributions from SM  $s$ -channel  $W$ -mediated and  $t$ -channel  $Z$ -mediated diagrams and a  $t$ -channel  $X$ -mediated diagram. As in the preceding paragraph, for  $i = j = \mu$  the  $W$ -mediated diagram is absent, whereas for  $j \neq i$  only the  $X$  contribution is present. It follows that from Eqs. (A1)-(A3) and (A5) we can derive the corresponding formulas for  $\bar{\nu}_i e^- \rightarrow \bar{\nu}_i e^-$  and  $\bar{\nu}_i e \rightarrow \bar{\nu}_j e$  with  $i \neq j$ , respectively, by simply interchanging  $s$  and  $u$ , assuming  $s < m_W^2$ . From the  $\bar{\nu}e$  counterpart of Eq.(A7), it is straightforward to obtain the minimum energy of the incident antineutrino [57]

$$2E_{\bar{\nu}}^{\min} = T + \sqrt{2m_e T + T^2} \tag{A8}$$

for a given  $T$ .

For the  $e^+ e^- \rightarrow \bar{\nu} \nu \gamma$  scattering, the amplitude receives contributions from five tree-level diagrams in the SM, three of which are mediated by the  $W$  and two by the  $Z$ , and from two  $X$ -mediated diagrams similar to the  $Z$  diagrams, with the final-state photon being attached to the  $e^\pm$  and  $W$  lines. The invariant kinematical variables can be chosen to be [43]

$$\hat{s} = (p_{e^+} + p_{e^-})^2 , \quad \hat{t} = (p_{e^+} - p_\nu)^2 , \quad \hat{u} = (p_{e^+} - p_{\bar{\nu}})^2 , \tag{A9}$$

$$\hat{s}' = (p_{\bar{\nu}} + p_\nu)^2 , \quad \hat{t}' = (p_{e^-} - p_\nu)^2 , \quad \hat{u}' = (p_{e^-} - p_{\bar{\nu}})^2 , \tag{A10}$$

$$\kappa_+ = 2p_{e^+} \cdot p_\gamma , \quad \kappa_- = 2p_{e^-} \cdot p_\gamma , \quad \kappa'_+ = 2p_{\bar{\nu}} \cdot p_\gamma , \quad \kappa'_- = 2p_\nu \cdot p_\gamma , \tag{A11}$$

where  $p_{e^\pm}$  are the four-momenta of  $e^\pm$ , etc. Averaging (summing) the absolute square of the amplitude over initial (final) spins and including all neutrino flavors, one then finds the contributions to the cross section in Eq. (12)

$$\begin{aligned} \overline{|\mathcal{M}_{e\bar{e}\rightarrow\nu_e\bar{\nu}_e\gamma}|^2} &= \frac{e^2 g^4}{2\kappa_- \kappa_+} \left\{ \left[ \left| 2\mathcal{G}_L^{ee} + \frac{1}{\mathcal{W}} \right|^2 \hat{u}^2 + \left| 2\mathcal{G}_L^{ee} + \frac{1}{\mathcal{W}'} \right|^2 \hat{u}'^2 + |2\mathcal{G}_R^{ee}|^2 (\hat{t}^2 + \hat{t}'^2) \right] \hat{s}' \right. \\ &\quad - \text{Re} \left[ \left( 2\mathcal{G}_L^{ee} + \frac{1}{\mathcal{W}} \right)^* \frac{\kappa_- \hat{s}' - \kappa'_+ \hat{t}' + \kappa'_- \hat{u}' + 4i \epsilon_{\eta\rho\tau\omega} p_{e^-}^\eta p_{\nu}^\rho p_{\bar{\nu}}^\tau p_\gamma^\omega}{\mathcal{W}\mathcal{W}'} \right] u^2 \\ &\quad - \text{Re} \left[ \left( 2\mathcal{G}_L^{ee} + \frac{1}{\mathcal{W}'} \right)^* \frac{\kappa_+ \hat{s}' - \kappa'_- \hat{t} + \kappa'_+ \hat{u} + 4i \epsilon_{\eta\rho\tau\omega} p_{e^+}^\eta p_{\nu}^\rho p_{\bar{\nu}}^\tau p_\gamma^\omega}{\mathcal{W}\mathcal{W}'} \right] u'^2 \\ &\quad \left. - \frac{\kappa_- \kappa'_+ \hat{t}' \hat{u}^2 + \kappa_+ \kappa'_- \hat{t} \hat{u}'^2}{|\mathcal{W}\mathcal{W}'|^2} \right\}, \end{aligned} \quad (\text{A12})$$

$$\overline{|\mathcal{M}_{e\bar{e}\rightarrow\nu_j\bar{\nu}_j\gamma}|^2} = \frac{2e^2 g^4}{\kappa_- \kappa_+} \left[ |\mathcal{G}_L^{jj}|^2 (\hat{u}^2 + \hat{u}'^2) + |\mathcal{G}_R^{jj}|^2 (\hat{t}^2 + \hat{t}'^2) \right] \hat{s}', \quad j = \mu, \tau, \quad (\text{A13})$$

$$\overline{|\mathcal{M}_{e\bar{e}\rightarrow\nu_j\bar{\nu}_l\gamma}|^2} = \frac{2e^2 g^4}{\kappa_- \kappa_+} \left[ |\mathcal{G}_L^{jl}|^2 (\hat{u}^2 + \hat{u}'^2) + |\mathcal{G}_R^{jl}|^2 (\hat{t}^2 + \hat{t}'^2) \right] \hat{s}', \quad j, l = e, \mu, \tau, \quad j \neq l, \quad (\text{A14})$$

where

$$\mathcal{W}^{(\prime)} = \hat{t}^{(\prime)} - m_W^2 + i\Gamma_W m_W, \quad (\text{A15})$$

$$\mathcal{G}_C^{ll'} = \frac{\delta_{ll'} \bar{g}_C}{2c_W^2 (\hat{s}' - m_Z^2 + i\Gamma_Z m_Z)} + \frac{C_{ll'}}{g^2 (\hat{s}' - m_X^2 + i\Gamma_X m_X)}, \quad C = L, R, \quad (\text{A16})$$

with  $\Gamma_W$  being the total width of  $W$ , etc. In the numerical analysis, we use  $\alpha = e^2/(4\pi) = 1/128$ ,  $G_F = g^2/(32 m_W^4)^{1/2} = 1.166 \times 10^{-5} \text{ GeV}^{-2}$ , and  $\sin^2 \theta_W = 0.23$ . With these parameters, we can reach most of the SM ranges listed in Table II to within 10%.

In our framework, the  $X$ -mediated amplitude for the flavor-changing decay  $\ell_i \rightarrow \ell_j e^+ e^-$  proceeds from a one-loop diagram for  $\ell_i \rightarrow \ell_j X^*$  involving internal  $W$ ,  $\nu_i$ , and  $\nu_j$  lines with  $X$  attached to the neutrino lines and eventually transforming into  $e^+ e^-$ . Since the masses of the external and internal leptons are small relative to  $m_W$ , it is a good approximation to retain only the lowest order terms in the small-mass expansion. In that limit, we can employ the results of Ref. [58] to derive

$$\mathcal{M}_{\ell_i \rightarrow \ell_j e^+ e^-} \sim \frac{G_F m_\nu^2 \ln(m_\nu^2/m_W^2)}{2\sqrt{2}\pi^2} \frac{\bar{\ell}_j \gamma^\lambda P_L \ell_i \bar{e} \gamma_\lambda (L_{ji} P_L + R_{ji} P_R) e}{\hat{s} - m_X^2 + i\Gamma_X m_X}, \quad (\text{A17})$$

after dropping a divergent term depending on the internal neutrino mass which in the complete model would be canceled by other contributions, assuming the presence of a GIM-like mechanism in the lepton sector of the model, and neglecting the final lepton masses. This implies that we only have an order-of-magnitude estimate of the decay branching ratio, given by

$$\mathcal{B}(\ell_i \rightarrow \ell_j e^+ e^-) \sim \frac{8G_F^2 m_\nu^4 \ln^2(m_\nu^2/m_W^2) (|L_{ji}|^2 + |R_{ji}|^2)}{3(4\pi)^7 \Gamma_{\ell_i} m_{\ell_i}^3} \int_0^{m_{\ell_i}^2} d\hat{s} \frac{(m_{\ell_i}^2 - \hat{s})^2 (m_{\ell_i}^2 + 2\hat{s})}{(\hat{s} - m_X^2)^2 + \Gamma_X^2 m_X^2}. \quad (\text{A18})$$

This is very suppressed for  $m_\nu < 1 \text{ eV}$ .

- 
- [1] J. Beringer *et al.* [Particle Data Group Collaboration], Phys. Rev. D **86**, 010001 (2012).
- [2] Z. Berezhiani and A. Rossi, Phys. Lett. B **535**, 207 (2002) [arXiv:hep-ph/0111137]; S. Davidson, C. Pena-Garay, N. Rius, and A. Santamaria, JHEP **0303**, 011 (2003) [arXiv:hep-ph/0302093].
- [3] J. Barranco, O.G. Miranda, C.A. Moura, and J.W.F. Valle, Phys. Rev. D **77**, 093014 (2008) [arXiv:0711.0698 [hep-ph]].
- [4] D.V. Forero and M.M. Guzzo, Phys. Rev. D **84**, 013002 (2011).
- [5] S.N. Gninenko and N.V. Krasnikov, Phys. Lett. B **513**, 119 (2001) [arXiv:hep-ph/0102222].
- [6] C. Boehm, Phys. Rev. D **70**, 055007 (2004) [arXiv:hep-ph/0405240].
- [7] A.W. Thomas, AIP Conf. Proc. **1418**, 147 (2011) [arXiv:1111.0122 [hep-ph]].
- [8] J. Erler and P. Langacker, in Ref. [1].
- [9] D. Hooper, Phys. Rev. D **75**, 123001 (2007) [arXiv:hep-ph/0701194].
- [10] P. Fayet, Phys. Rev. D **75**, 115017 (2007) [arXiv:hep-ph/0702176].
- [11] R. Foot, X.G. He, H. Lew, and R.R. Volkas, Phys. Rev. D **50**, 4571 (1994) [arXiv:hep-ph/9401250]; P.f. Yin, J. Liu, and S.h. Zhu, Phys. Lett. B **679**, 362 (2009) [arXiv:0904.4644 [hep-ph]].
- [12] X.G. He, J. Tandean, and G. Valencia, Phys. Lett. B **631**, 100 (2005) [arXiv:hep-ph/0509041]; C.H. Chen, C.Q. Geng, and C.W. Kao, Phys. Lett. B **663**, 400 (2008) [arXiv:0708.0937 [hep-ph]]; S. Oh and J. Tandean, JHEP **1001**, 022 (2010) [arXiv:0910.2969 [hep-ph]].
- [13] S. Oh and J. Tandean, Phys. Lett. B **697**, 41 (2011) [arXiv:1008.2153 [hep-ph]].
- [14] V.M. Abazov *et al.* [D0 Collaboration], Phys. Rev. D **82**, 032001 (2010) [arXiv:1005.2757 [hep-ex]]; Phys. Rev. Lett. **105**, 081801 (2010) [arXiv:1007.0395 [hep-ex]].
- [15] M. Pospelov, Phys. Rev. D **80**, 095002 (2009) [arXiv:0811.1030 [hep-ph]]; S. Oh and J. Tandean, Phys. Rev. D **83**, 095006 (2011) [arXiv:1102.1680 [hep-ph]].
- [16] M. Reece and L.T. Wang, JHEP **0907**, 051 (2009) [arXiv:0904.1743 [hep-ph]].
- [17] K. Nakamura and S.T. Petcov, in Ref. [1].
- [18] R.C. Allen *et al.*, Phys. Rev. D **47**, 11 (1993).
- [19] L.B. Auerbach *et al.* [LSND Collaboration], Phys. Rev. D **63**, 112001 (2001) [arXiv:hep-ex/0101039].
- [20] F. Reines, H.S. Gurr, and H.W. Sobel, Phys. Rev. Lett. **37**, 315 (1976).
- [21] G.S. Vidyakin *et al.*, JETP Lett. **55**, 206 (1992) [Pisma Zh. Eksp. Teor. Fiz. **55**, 212 (1992)].
- [22] A.I. Derbin *et al.*, JETP Lett. **57**, 796 (1993) [Pisma Zh. Eksp. Teor. Fiz. **57**, 755 (1993)].
- [23] Z. Daraktchieva *et al.* [MUNU Collaboration], Phys. Lett. B **564**, 190 (2003) [arXiv:hep-ex/0304011]; Phys. Lett. B **615**, 153 (2005) [arXiv:hep-ex/0502037].
- [24] M. Deniz *et al.* [TEXONO Collaboration], Phys. Rev. D **81**, 072001 (2010) [arXiv:0911.1597 [hep-ex]].
- [25] R. Beyer and G. Radcliff, Prog. Part. Nucl. Phys. **32**, 399 (1994).
- [26] P. Vilain *et al.* [CHARM-II Collaboration], Phys. Lett. B **335**, 246 (1994).
- [27] F. Boehm and P. Vogel, *Physics of Massive Neutrinos* (Cambridge University Press, Cambridge, 1987).
- [28] G. 't Hooft, Phys. Lett. B **37**, 195 (1971).
- [29] B. Kayser, E. Fischbach, S.P. Rosen, and H. Spivack, Phys. Rev. D **20**, 87 (1979).
- [30] D. Buskulic *et al.* [ALEPH Collaboration], Phys. Lett. B **384**, 333 (1996).
- [31] R. Barate *et al.* [ALEPH Collaboration], Phys. Lett. B **420**, 127 (1998) [arXiv:hep-ex/9710009].
- [32] R. Barate *et al.* [ALEPH Collaboration], Phys. Lett. B **429**, 201 (1998).
- [33] A. Heister *et al.* [ALEPH Collaboration], Eur. Phys. J. C **28**, 1 (2003).

- [34] P. Abreu *et al.* [DELPHI Collaboration], *Eur. Phys. J. C* **17**, 53 (2000) [arXiv:hep-ex/0103044].
- [35] J. Abdallah *et al.* [DELPHI Collaboration], *Eur. Phys. J. C* **38**, 395 (2005) [arXiv:hep-ex/0406019].
- [36] M. Acciarri *et al.* [L3 Collaboration], *Phys. Lett. B* **415**, 299 (1997).
- [37] M. Acciarri *et al.* [L3 Collaboration], *Phys. Lett. B* **444**, 503 (1998).
- [38] M. Acciarri *et al.* [L3 Collaboration], *Phys. Lett. B* **470**, 268 (1999) [arXiv:hep-ex/9910009].
- [39] K. Ackerstaff *et al.* [OPAL Collaboration], *Eur. Phys. J. C* **2**, 607 (1998) [arXiv:hep-ex/9801024].
- [40] G. Abbiendi *et al.* [OPAL Collaboration], *Eur. Phys. J. C* **8**, 23 (1999) [arXiv:hep-ex/9810021].
- [41] G. Abbiendi *et al.* [OPAL Collaboration], *Eur. Phys. J. C* **18**, 253 (2000) [arXiv:hep-ex/0005002].
- [42] E. Ma and J. Okada, *Phys. Rev. Lett.* **41**, 287 (1978) [Erratum-*ibid.* **41**, 1759 (1978)]; K.J.F. Gaemers, R. Gastmans, and F.M. Renard, *Phys. Rev. D* **19**, 1605 (1979).
- [43] F.A. Berends, G.J.H. Burgers, C. Mana, M. Martinez, and W.L. van Neerven, *Nucl. Phys. B* **301**, 583 (1988).
- [44] S. Godfrey, P. Kalyniak, B. Kamal, and A. Leike, *Phys. Rev. D* **61**, 113009 (2000) [arXiv:hep-ph/0001074].
- [45] T.A. Mueller *et al.*, *Phys. Rev. C* **83**, 054615 (2011) [arXiv:1101.2663 [hep-ex]].
- [46] M. Williams, C.P. Burgess, A. Maharana, and F. Quevedo, *JHEP* **1108**, 106 (2011) [arXiv:1103.4556 [hep-ph]].
- [47] C.W. Chiang, Y.F. Lin, and J. Tandean, *JHEP* **1111**, 083 (2011) [arXiv:1108.3969 [hep-ph]].
- [48] C.D. Carone and H. Murayama, *Phys. Rev. Lett.* **74**, 3122 (1995) [hep-ph/9411256]; *Phys. Rev. D* **52**, 484 (1995) [hep-ph/9501220]; E. Ma and D.P. Roy, *Phys. Rev. D* **58**, 095005 (1998) [hep-ph/9806210].
- [49] J.P. Leveille, *Nucl. Phys. B* **137**, 63 (1978).
- [50] T. Aoyama, M. Hayakawa, T. Kinoshita, and M. Nio, *Phys. Rev. Lett.* **109**, 111807 (2012) [arXiv:1205.5368 [hep-ph]].
- [51] H. Merkel *et al.* [A1 Collaboration], *Phys. Rev. Lett.* **106**, 251802 (2011) [arXiv:1101.4091 [nucl-ex]]; S. Abrahamyan *et al.* [APEX Collaboration], *Phys. Rev. Lett.* **107**, 191804 (2011) [arXiv:1108.2750 [hep-ex]].
- [52] J.D. Bjorken, R. Essig, P. Schuster, and N. Toro, *Phys. Rev. D* **80**, 075018 (2009) [arXiv:0906.0580 [hep-ph]].
- [53] S. Andreas, C. Niebuhr, and A. Ringwald, *Phys. Rev. D* **86**, 095019 (2012) [arXiv:1209.6083 [hep-ph]].
- [54] M. Freytsis, G. Ovanesyan, and J. Thaler, *JHEP* **1001**, 111 (2010) [arXiv:0909.2862 [hep-ph]].
- [55] D. Buskulic *et al.* [ALEPH Collaboration], *Z. Phys. C* **66**, 3 (1995).
- [56] A. Pukhov *et al.*, hep-ph/9908288.
- [57] J.N. Bahcall, *Phys. Rev.* **136**, B1164 (1964).
- [58] X.G. He, J. Tandean, and G. Valencia, *Eur. Phys. J. C* **64**, 681 (2009) [arXiv:0909.3638 [hep-ph]].
- [59] M. Hirsch, E. Nardi, and D. Restrepo, *Phys. Rev. D* **67**, 033005 (2003) [arXiv:hep-ph/0210137].

TABLE II: Measured and SM values of  $e^+e^- \rightarrow \nu\bar{\nu}\gamma$  cross section for various  $e^+e^-$  center-of-mass energies and cuts on  $E_\gamma$ ,  $x = 2E_\gamma/\sqrt{s}$ ,  $x_T = x \sin \theta_\gamma$ , or  $E_{\gamma T} = \sqrt{s} x_T/2$  and  $\hat{y} = \cos \theta_\gamma$ . The second (third) number in each  $\sigma_{\text{exp}}$  entry is the statistical (systematic) error. The  $\sigma_{\text{SM}}$  entries are available from the experimental papers. Most of these numbers were previously quoted in Refs. [3, 4, 59].

|             | $\sqrt{s}$ (GeV)         | $\sigma_{\text{exp}}$ (pb) | $\sigma_{\text{SM}}$ (pb) | $E_\gamma, x, x_T, \hat{y}$ cuts                         |
|-------------|--------------------------|----------------------------|---------------------------|--|
| ALEPH [30]  | 130.0                    | $9.6 \pm 2.0 \pm 0.3$      | $10.7 \pm 0.2$            | } $E_\gamma \geq 10 \text{ GeV},  \hat{y}  \leq 0.95$    |
|             | 136.0                    | $7.2 \pm 1.7 \pm 0.2$      | $9.1 \pm 0.2$             |  |
|             | [31] 161.0               | $5.3 \pm 0.8 \pm 0.2$      | $5.81 \pm 0.03$           | } $x_T \geq 0.075,  \hat{y}  \leq 0.95$                  |
|             | 172.0                    | $4.7 \pm 0.8 \pm 0.2$      | $4.85 \pm 0.04$           |  |
|             | [32] 182.7               | $4.32 \pm 0.31 \pm 0.13$   | $4.15 \pm 0.03$           |  |
|             | [33] 188.6               | $3.43 \pm 0.16 \pm 0.06$   | $3.48 \pm 0.05$           |  |
|             | 191.6                    | $3.47 \pm 0.39 \pm 0.06$   | $3.23 \pm 0.05$           |  |
|             | 195.5                    | $3.03 \pm 0.22 \pm 0.06$   | $3.26 \pm 0.05$           |  |
|             | 199.5                    | $3.23 \pm 0.21 \pm 0.06$   | $3.12 \pm 0.05$           |  |
|             | 201.6                    | $2.99 \pm 0.29 \pm 0.05$   | $3.07 \pm 0.05$           |  |
|             | 205.0                    | $2.84 \pm 0.21 \pm 0.05$   | $2.93 \pm 0.05$           |  |
| 206.7       | $2.67 \pm 0.16 \pm 0.05$ | $2.80 \pm 0.05$            |                           |  |
| DELPHI [34] | 182.7                    | $1.85 \pm 0.25 \pm 0.15$   | $2.04 \pm 0.02$           | } $x \geq 0.06,  \hat{y}  \leq 0.707$                    |
|             | 188.7                    | $1.80 \pm 0.15 \pm 0.14$   | $1.97 \pm 0.02$           |  |
|             | 182.7                    | $2.33 \pm 0.31 \pm 0.19$   | $2.08 \pm 0.02$           | } $0.2 \leq x \leq 0.9, 0.848 \leq  \hat{y}  \leq 0.978$ |
|             | 188.7                    | $1.89 \pm 0.16 \pm 0.15$   | $1.94 \pm 0.02$           |  |
|             | 182.7                    | $1.27 \pm 0.25 \pm 0.11$   | $1.50 \pm 0.02$           | } $0.3 \leq x \leq 0.9, 0.990 \leq  \hat{y}  \leq 0.998$ |
|             | [35] 188.7               | $1.41 \pm 0.15 \pm 0.13$   | $1.42 \pm 0.01$           |  |
|             | 187.1                    | $1.37 \pm 0.14 \pm 0.11$   | $1.44 \pm 0.01$           |  |
|             | 196.8                    | $1.22 \pm 0.14 \pm 0.10$   | $1.29 \pm 0.01$           |  |
|             | 205.4                    | $1.12 \pm 0.11 \pm 0.09$   | $1.18 \pm 0.01$           | } $0.2 \leq x \leq 0.9, 0.848 \leq  \hat{y}  \leq 0.978$ |
|             | 187.1                    | $1.98 \pm 0.14 \pm 0.16$   | $1.97 \pm 0.02$           |  |
|             | 196.8                    | $1.71 \pm 0.14 \pm 0.14$   | $1.76 \pm 0.02$           |  |
|             | 205.4                    | $1.71 \pm 0.12 \pm 0.14$   | $1.57 \pm 0.02$           | } $x \geq 0.06,  \hat{y}  \leq 0.707$                    |
|             | 187.1                    | $1.78 \pm 0.13 \pm 0.16$   | $1.89 \pm 0.02$           |  |
| 196.8       | $1.41 \pm 0.13 \pm 0.13$ | $1.75 \pm 0.02$            |                           |  |
| 205.4       | $1.50 \pm 0.11 \pm 0.14$ | $1.61 \pm 0.02$            |                           |  |
| L3 [36]     | 161.3                    | $6.75 \pm 0.91 \pm 0.18$   | $6.26 \pm 0.12$           | } $E_{\gamma T} \geq 6 \text{ GeV},  \hat{y}  \leq 0.97$ |
|             | 172.3                    | $6.12 \pm 0.89 \pm 0.14$   | $5.61 \pm 0.10$           |  |
|             | [37] 182.7               | $5.36 \pm 0.39 \pm 0.10$   | $5.62 \pm 0.10$           | } $E_\gamma \geq 5 \text{ GeV},  \hat{y}  \leq 0.97$     |
|             | [38] 188.6               | $5.25 \pm 0.22 \pm 0.07$   | $5.28 \pm 0.05$           |  |
| OPAL [39]   | 130.3                    | $10.0 \pm 2.3 \pm 0.4$     | $13.48 \pm 0.22$          | } $x_T \geq 0.05,  \hat{y}  \leq 0.82$                   |
|             | 136.2                    | $16.3 \pm 2.8 \pm 0.7$     | $11.30 \pm 0.20$          |  |
|             | 161.3                    | $5.3 \pm 0.8 \pm 0.2$      | $6.49 \pm 0.08$           |  |
|             | 172.1                    | $5.5 \pm 0.8 \pm 0.2$      | $5.53 \pm 0.08$           | } $x_T \geq 0.1, 0.82 \leq  \hat{y}  \leq 0.966$         |
|             | [40] 130.0               | $11.6 \pm 2.5 \pm 0.4$     | $14.26 \pm 0.06$          |  |
|             | 136.0                    | $14.9 \pm 2.4 \pm 0.5$     | $11.95 \pm 0.07$          | } $x_T \geq 0.05,  \cos \theta_\gamma  \leq 0.966$       |
|             | 182.7                    | $4.71 \pm 0.34 \pm 0.16$   | $4.98 \pm 0.02$           |  |
|             | [41] 188.6               | $4.35 \pm 0.17 \pm 0.09$   | $4.66 \pm 0.03$           |  |